1982-06

A study of east-coast cyclogenesis employing quasi-lagrangian diagnostics.

Conant, Peter R.

Monterey, California. Naval Postgraduate School

NAVAL POSTGRADUATE SCHOOL
Monterey, California

THESIS

A STUDY OF EAST-COAST CYCLOGENESIS
EMPLOYING QUASI-LAGRANGIAN DIAGNOSTICS

by

Peter R. Conant

June 1982

Thesis Advisor: C. H. Wash

Approved for public release; distribution unlimited

SECURITY CLASSIFICATION OF THIS PAGE (When Data Entered)

REPORT DOCUMENTATION PAGE

READ INSTRUCTIONS BEFORE COMPLETING FORM

1. REPORT NUMBER	2. GOVT ACCESSION NO. / 3. RECIPIENT'S CATALOG NUMBER
4. TITLE (and Subtitle): A Study of East-Coast Cyclogenesis Employing Quasi-Lagrangian Diagnostics	5. TYPE OF REPORT & PERIOD COVERED: Master's Thesis; June 1982
	6. PERFORMING ORG. REPORT NUMBER
7. AUTHOR(s): Peter R. Conant	8. CONTRACT OR GRANT NUMBER(s)
9. PERFORMING ORGANIZATION NAME AND ADDRESS: Naval Postgraduate School, Monterey, California 93940	10. PROGRAM ELEMENT, PROJECT, TASK AREA & WORK UNIT NUMBERS
11. CONTROLLING OFFICE NAME AND ADDRESS: Naval Postgraduate School, Monterey, California 93940	12. REPORT DATE: June 1982
	13. NUMBER OF PAGES: 102
14. MONITORING AGENCY NAME & ADDRESS(if different from Controlling Office)	15. SECURITY CLASS. (of this report): Unclassified
	15a. DECLASSIFICATION/DOWNGRADING SCHEDULE

16. DISTRIBUTION STATEMENT (of this Report)

Approved for public release; distribution unlimited

17. DISTRIBUTION STATEMENT (of the abstract entered in Block 20, if different from Report)

18. SUPPLEMENTARY NOTES

19. KEY WORDS (Continue on reverse side if necessary and identify by block number)

absolute vorticity, absolute angular momentum, Presidents' Day Cyclone, quasi-Lagrangian diagnostics, budgets, First GARP Global Experiment, explosive maritime cyclogenesis

20. ABSTRACT (Continue on reverse side if necessary and identify by block number)

The absolute vorticity and angular momentum budgets for the Presidents' Day Cyclone, 18-19 February 1979 are evaluated employing the quasi-Lagrangian diagnostic technique in pressure coordinates. The First GARP Global Experiment (FGGE) Level III-b data set prepared by the European Center for Medium Range Weather Forecasts is used to define the storm and to calculate the budgets.

Important differences are found between the FGGE and mass

DD FORM 1 JAN 73 1473 EDITION OF 1 NOV 68 IS OBSOLETE
S/N 0102-014-6601

SECURITY CLASSIFICATION OF THIS PAGE (When Data Entered)

budget vertical motion estimates. The budget results illustrate the importance of inward eddy mode lateral transport and advection at upper levels and mean mode transport due to convergence at lower levels. The vertical redistribution plays a lesser role but is more significant in the angular momentum budget. The vertical vorticity advection and tilting terms are comparable in magnitude. The largest budget residuals occur during the period of most intense convective activity which indicates a need for a better understanding of the vertical redistribution processes.

Approved for public release; distribution unlimited

A Study of East-Coast Cyclogenesis Employing Quasi-Lagrangian Diagnostics

by

Peter R. Conant
Captain, United States Air Force
B.S., North Carolina State University, 1976

Submitted in partial fulfillment of the
requirements for the degree of

MASTER OF SCIENCE IN METEOROLOGY

from the

NAVAL POSTGRADUATE SCHOOL
June 1982

ABSTRACT

The absolute vorticity and angular momentum budgets for the Presidents' Day Cyclone, 18-19 February 1979 are evaluated employing the quasi-Lagrangian diagnostic technique in pressure coordinates. The First GARP Global Experiment (FGGE) Level III-b data set prepared by the European Center for Medium Range Weather Forecasts is used to define the storm and to calculate the budgets.

Important differences are found between the FGGE and mass budget vertical motion estimates. The budget results illustrate the importance of inward eddy mode lateral transport and advection at upper levels and mean mode transport due to convergence at lower levels. The vertical redistribution plays a lesser role but is more significant in the angular momentum budget. The vertical vorticity advection and tilting terms are comparable in magnitude. The largest budget residuals occur during the period of most intense convective activity which indicates a need for a better understanding of the vertical redistribution processes.

TABLE OF CONTENTS

LIST OF TABLES

LIST OF FIGURES

ACKNOWLEDGEMENT

The development of this thesis would have been virtually impossible without the guidance and encouragement provided by Dr. Carlyle H. Wash. The author expresses heartfelt appreciation for his immeasurable contributions as the thesis advisor.

Additionally, the author wishes to thank Dr. Russell Elsberry for his many recommendations, both scientific and editorial, in his role as second reader. His immediate attention to the successive drafts of this document is especially appreciated. A special thanks goes to Michael McDermet for his help in the graphics preparation. Also, the author expresses appreciation to CAPT Alan R. Shaffer for the many instances in which he clarified meteorological concepts and to the Department of Meteorology faculty members whose previous instruction proved invaluable in the completion of this study.

I. INTRODUCTION

Operational forecast models have generally performed poorly in predicting the frequently observed, cold-season explosive cyclogenesis of maritime cyclones. Sanders and Gyakum (1980) demonstrated that the National Meteorological Center's (NMC) Limited Area Fine-Mesh Model (LFM) predicts only one-fourth to one-third of the deepening rates of rapidly deepening maritime cyclones.

The accurate forecasting of these meteorological events over the open ocean, as well as in coastal regions, is of critical importance to both civilian and military interests. The extreme conditions produced by these storms often result in loss of life, destruction of property and disruption of operations. The recent sinking of the oil rig Ocean Ranger (LeMoyne, 1982) and the attendant loss of life illustrates the magnitude of the destructive forces created by intense maritime cyclones. Throughout recorded history, these storms have claimed numerous ocean-going vessels in preferred areas of explosive cyclogenesis such as off the east coast of the U.S. These cyclones often strike with little or no warning. More accurate and timely forecasting of explosively developing maritime cyclones would undoubtedly reduce their impact on human activity.

The failure of numerical forecast models in predicting the intensities of vigorous maritime cyclones is due to the small scales over which the explosive development occurs as well as the lack of meteorological observations over oceanic areas. This problem has resulted in an inaccurate representation of the initial conditions in the forecast models. The most promising solution to this problem is the incorporation of wind, temperature, moisture and pressure data obtained from satellite measurements in the operational prediction models. It appears however, that a better understanding of the role of dynamic forcing in maritime cyclogenesis is required if this new data source is to be fully utilized.

This study constitutes a portion of a broad-based research effort to better understand the processes leading to the development, maturation and decay of extratropical maritime cyclones. This improved understanding will point toward ways to improve the numerical prediction of maritime cyclogenesis.

More specifically, this thesis consists of circulation (vorticity) and angular momentum budget analyses of the Presidents' Day Cyclone (18-19 February 1979); a subsynoptic

scale event which provided a well-defined example of explosive maritime cyclogenesis. This storm has been the subject of several in-depth analyses (Bosart, 1981; Roman, 1981; Uccellini, Kocin and Wash, 1981). It produced record breaking snowfalls (nearly 60 cm) in portions of Virginia, Maryland and Delaware. The central surface pressure decreased by more than 27 mb during a 24-hour period. The NMC LFM-II model underforecast the decrease in the surface pressure minimum by an average of 8 to 16 mb during the explosive cyclogenesis period (Bosart, 1981). Thus, the Presidents' Day Cyclone can be included in a class of explosive deepeners not adequately handled by current numerical forecast models (Sanders and Gyakum, 1980). This cyclone developed during one of the First GARP Global Experiment (FGGE) special observing periods. Consequently, there are additional observational data and research-based objective analyses to aid in the study.

Roman (1981) completed a mass budget study of the Presidents' Day Cyclone based on the FGGE data set. He computed vertical velocity values in layers consistent with the lateral mass transport and time tendency terms. The vertical velocity fields in the FGGE data set are used to compute the

vertical transport terms in the budget studies in this thesis.

Quasi-Lagrangian diagnostic (QLD) procedures (Wash, 1978) are employed in this study. The basic feature of the QLD budget approach is the computation of volume integrals of atmospheric properties. This volume is centered on and moved with the surface pressure minimum of the Presidents' Day Cyclone. This approach incorporates the translational effects associated with the cyclone, as well as the effects due to development or decay. The lateral exchanges, sources and sinks, and vertical redistributions of meteorological variables are primarily the result of developmental processes. QLD budgets yield quantitative evaluations of the exchanges of mass, circulation, angular momentum and kinetic energy between the budget volume and its environment.

The circulation about the surface cyclone increases dramatically during cyclogenesis, and provides a convenient measure of cyclone intensity. The circulation budget is used to evaluate the magnitude of the divergence and horizontal and vertical advection terms in the vorticity equation. It is well known that upper-level vorticity advection contributes to cyclogenetic processes via the divergence and

vertical velocity fields (Petterssen, 1956). This qualitative relationship does not however, provide answers to key questions such as:

- What is the magnitude and significance of low-level horizontal vorticity advection?
- How does the vertical advection of vorticity contribute to cyclogenesis?
- What is the magnitude of the local generation of vorticity?

The quantitative analysis of circulation using budget diagnostics provides answers to these questions through the identification of lateral exchanges, vertical redistributions and sources and sinks.

An alternative, but closely related, measure of vortex intensity is that of angular momentum. The concentration of momentum about the storm axis is primarily the result of radial transport. Johnson and Downey (1975) show that there are no sources of angular momentum within the moving budget volume. Large scale forcing of storm angular momentum buildup occurs through inward transport of angular momentum at lower levels. One objective of the QLD analysis of angular momentum is to reveal the significance of the vertical transport of this property during the development of the Presidents' Day Cyclone.

The budget analyses are done in isobaric vertical coordinates. The choice of these coordinates is made for convenience in comparing the budget analyses with standard diagnostic and prognostic charts. These analyses can also be converted to sigma vertical coordinates over level terrain to facilitate comparisons with results from numerical model predictions.

In summary, the purpose of this thesis is to examine a well-defined maritime cyclogenesis event in terms of circulation and angular momentum from the budget perspective. The specific objectives of this study are:

- Quantitatively evaluate the horizontal transport, vertical redistribution and sources/sinks of vorticity and angular momentum within a budget volume centered on the Presidents' Day Cyclone;
- Compare the vertical velocity structure of the Presidents' Day Cyclone derived from the mass budget vertical transport (Roman, 1981) with that of the FGGE data set.

A brief description of the FGGE data set and a synoptic overview of the Presidents' Day Cyclone are presented in the following chapter. Chapter III contains an abbreviated description of the QLD technique. A more detailed explanation of the quasi-Lagrangian coordinate system and generalized budget equations is presented in Appendix B. The results of the budget analyses are presented in Chapter IV.

Chapter V contains the conclusions of this study and recommendations for further research.

II. DATA BASE AND SYNOPTIC OVERVIEW

A. DATA BASE

The synoptic descriptions and budget analyses of the Presidents' Day Cyclone are based solely on the FGGE Level III-b data set. More specifically, FGGE analyses between 1200 GMT 18 February and 1200 GMT 20 February 1979 are used to define the development and movement of this storm. The FGGE analyses were prepared by the European Center for Medium Range Weather Forecasts (ECMWF) using a three-dimensional optimal interpolation scheme on a high resolution (1.875 degrees of latitude and longitude) nonstaggered grid. This nonlinear analysis scheme produced high-quality, vertically and horizontally consistent mass and momentum fields. A more detailed description of the analysis scheme is found in the Global Weather Experiment, The Daily Global Analysis, Part 1, (1981), published by ECMWF.

The validity of the FGGE data set in defining the Presidents' Day Cyclone was demonstrated by Roman (1981). His subjective comparisons with the Bosart (1981) analyses, the Fleet Numerical Oceanography Center analyses and the NMC LFM

analyses clearly illustrate the accuracy of the FGGE data in representing the atmospheric conditions during the period.

Some of the advantages in using the FGGE data set as opposed to conventional analyses are:

- The incorporation of a variety of data sources including off-time and late data;
- The high resolution regular grid is particularly useful in examining the subsynoptic scale features of the Presidents' Day Cyclone;
- The data set includes several derived fields such as relative humidity and vertical velocity;
- The analyses fully encompass the area of development and movement of the Presidents' Day Cyclone.

The FGGE Level III-b data set includes fields of pressure height, u and v wind components, temperature and vertical velocity for all standard pressure levels and relative humidity for all standard levels up to 300mb (Table I). Additionally, absolute vorticity and thickness fields were derived for use in this thesis.

B. SYNOPTIC OVERVIEW

The purpose of this section is to review the changes in the mass and momentum fields over the eastern U.S. and western Atlantic that led to the development of the Presidents' Day Cyclone. This review differs from previous discussions of the storm (Bosart, 1981; and Uccellini, Kocin and Wash,

1981) by focusing on these changes in relation to the budget volume translating with the surface pressure minimum. The discussion is based on the pressure, temperature and wind analyses and the derived vorticity and thickness fields from the FGGE data set. The discussion in terms of vorticity and thermal advection serves to provide a background for the circulation and angular momentum budget study analyses presented in Chapter IV.

All of the synoptic figures in this thesis depict budget volumes with lateral boundaries at six and nine degrees latitude. The six-degree boundary was selected because it generally includes the intense part of the storm. The nine-degree boundary was chosen since it encompasses nearly all of the peripheral features related to the storm. The six and nine degree circles are referred to throughout this section as the inner and outer boundaries. The circular representation of the budget volume lateral boundaries introduces a small distortion since these boundaries should be slightly elliptical on the conformal projections used in the figures. Also, the position of the budget volume at 1200 GMT 18 February is based on the first distinguishable surface pressure minimum of the Presidents' Day Cyclone (not shown).

TABLE I

FGGE LEVEL III-b DATA FIELDS FOR TIMES SHOWN BELOW

SURFACE PRESSURE FIELDS ARE ALSO AVAILABLE

LEVEL (mb x 10) =	100	85	70	50	40	30	25	20	15	10
PRESSURE HEIGHTS	X	X	X	X	X	X	X	X	X	X
VERTICAL VELOCITY	X	X	X	X	X	X	X	X	X	X
RELATIVE HUMIDITY	X	X	X	X	X	X				
TEMPERATURE	X	X	X	X	X	X	X	X	X	X
U WIND COMPONENTS	X	X	X	X	X	X	X	X	X	X
V WIND COMPONENTS	X	X	X	X	X	X	X	X	X	X

TIME PERIODS AVAILABLE (GMT)

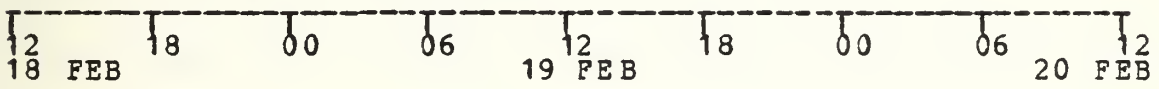

Figure 1 depicts the 6-hourly positions of the storm's surface pressure minima prior to, during and following the period of explosive cyclogenesis from 0000 GMT 19 February through 0000 GMT 20 February 1979. During this time, the surface pressure minima decreased by 27 mb for an average deepening rate in excess of 1 mb per hour for 24 hours. The

maximum 6-hour decrease was 10.3 mb between 1200 GMT and 1800 GMT 19 February. Figs. 2 through 6 depict the surface pressure patterns and the 850 and 500mb height contours and isotherms at 12-hour intervals from 1200 GMT 18 February through 1200 GMT 20 February. The 1000mb thermal fields appear with the surface pressure patterns since the surface temperature fields are not included in the FGGE Level-IIIb data set. The 500mb wind vectors and absolute vorticity fields at 12-hour intervals are presented in Figs. 7 and 8. The examination of these figures yields qualitative estimates of mid-level vorticity advection. Finally, the 1000-500mb thickness patterns and 1000mb height contours appear in Figs. 9 and 10. These figures are useful in determining lower tropospheric thermal advection.

At 1200 GMT 18 February the dominant surface synoptic feature is a massive cold high pressure system centered over northern New York with a ridge to the south over and east of the Appalachians (Fig. 2a). This ridge is a hydrostatic reflection of the shallow cold air entrenched east of the Appalachians. The thermal trough at the 1000mb level in this region is located within the northwestern portion of the outer budget volume boundary. Another feature of interest

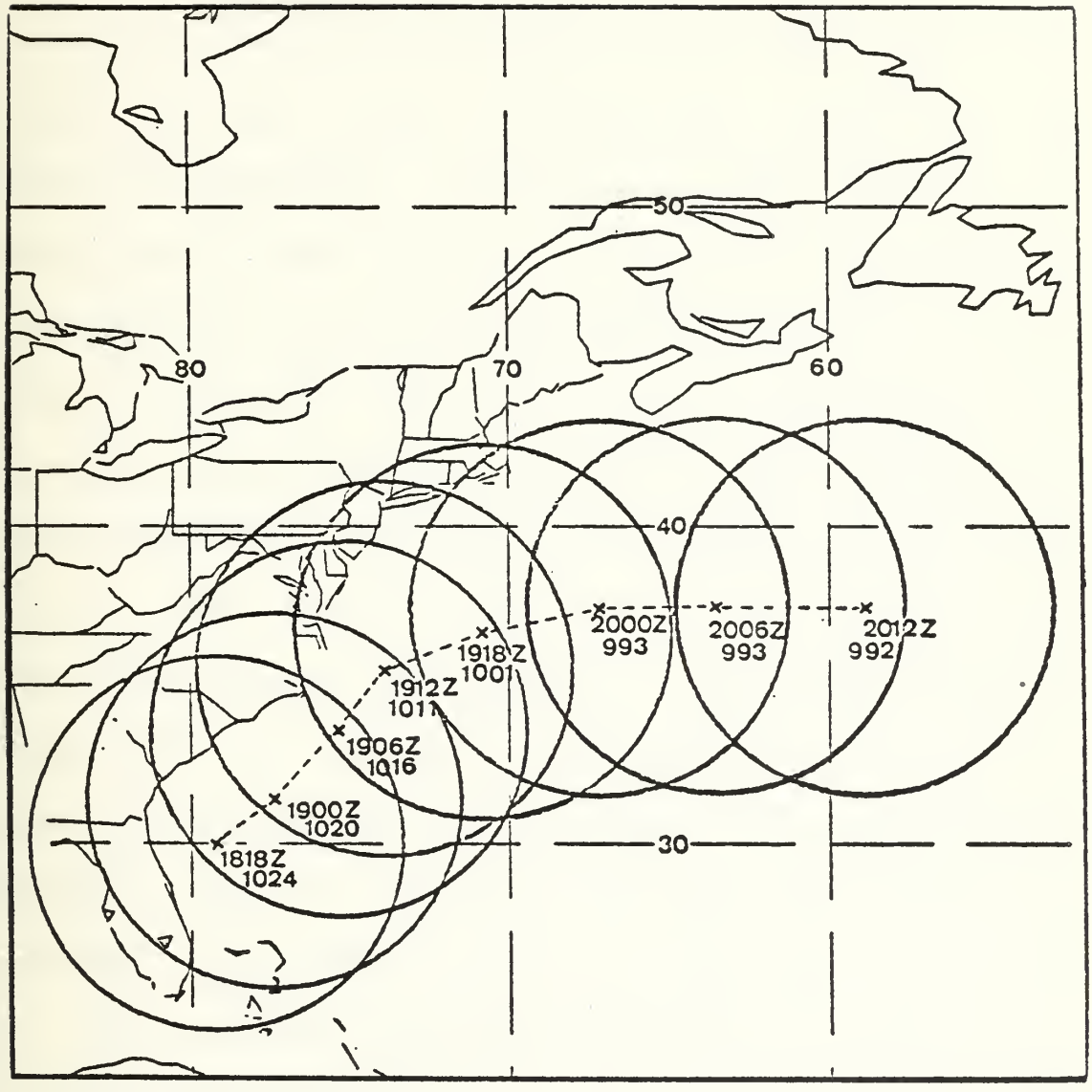

Figure 1. Presidents Day Cyclone track at 6-hour intervals from 1800 GMT 18 February through 1200 GMT 20 February, 1979 with 6 degree radius circles. Times are date and hour in GMT (Z). Central surface pressures in mb appear below times.

at the surface is the inverted pressure trough in the central Gulf of Mexico. Additionally, a weak trough is seen near the center of the budget volume. The 850 mb contour pattern (Fig. 2b) shows a strong ridge over the northeastern states that extends into the Great Lakes region, and a sharp trough from North Dakota southeastward across the inner budget volume boundary. The 850mb isotherm pattern is primarily zonal in the vicinity of the budget volume with little indication of the underlying shallow cold air. The key feature at the 500mb level (Fig. 2c) is a short wave embedded in a nearly zonal flow across the upper Midwest. The wave is generally in phase with the thermal trough at this level. A weak ridge is seen in the 500mb contour pattern north of the inner volume boundary. The absolute vorticity maximum (Fig. 7a) extends into the northern portion of the budget volume and southward into Texas. Positive vorticity advection (PVA) is occurring to the west and northwest of the budget volume from Illinois southwestward into Louisiana. The 1000-500mb thickness pattern (Fig. 9a) indicates a broad area of strong cold advection throughout the lower troposphere over the western North Atlantic. Weak cold advection is present across the northeastern budget volume boundary.

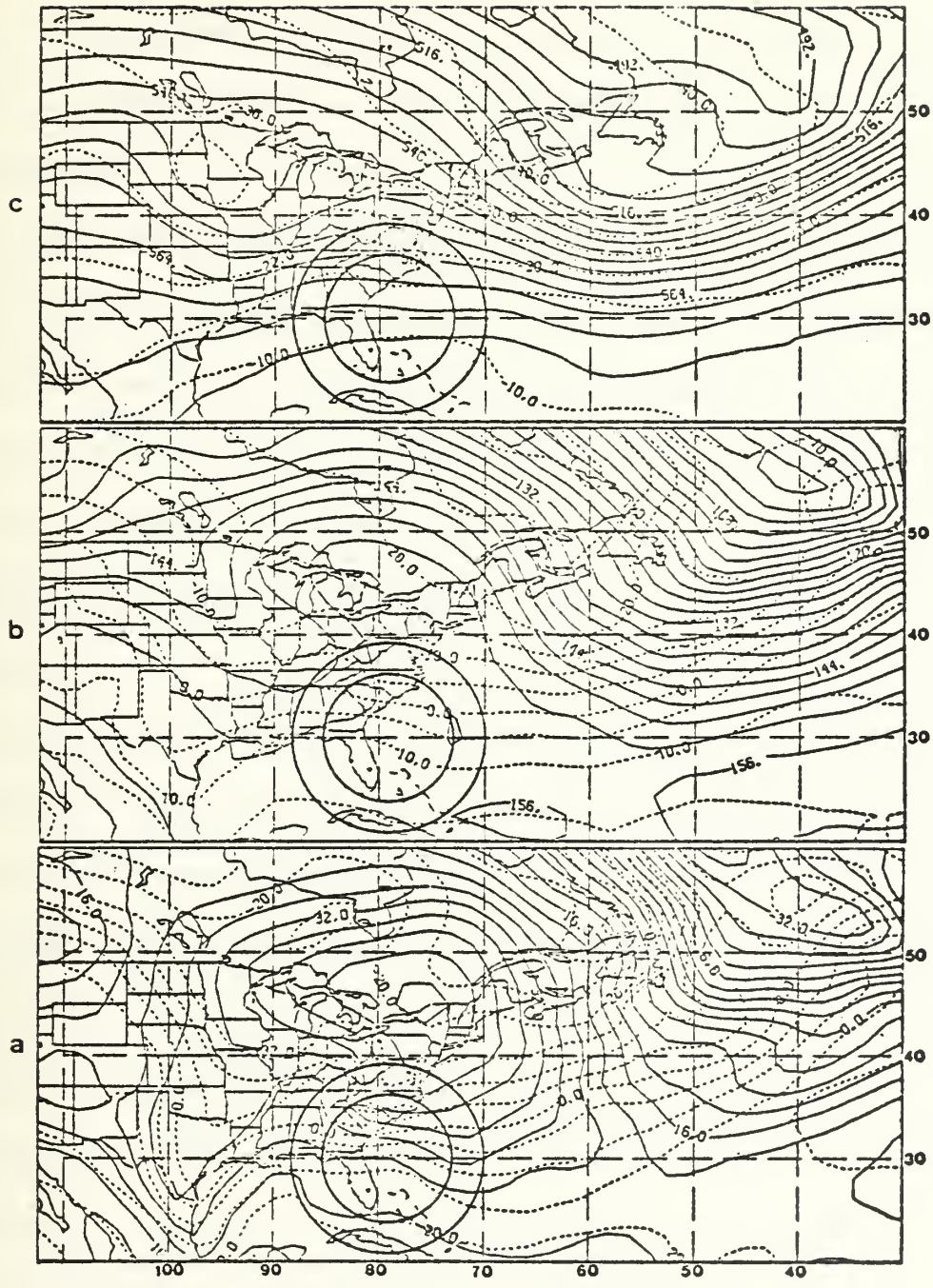

Figure 2. a. Surface pressure and 1000mb isotherms, b. 850mb height contours and isotherms and c. 500mb contours and isotherms for 1200 GMT 18 February 1979. Surface pressure is p-1000mb. Contours are labeled in decameters and isotherms (°C) are dashed. Circles are 6 and 9 degree budget volume lateral boundaries.

Significant changes occur in the low-level patterns during the 12 hour period ending at 0000 GMT 19 February. The surface high pressure center (Fig. 3a) moves southeastward to Massachusetts. More importantly, however, is the development of a cyclonic circulation off the coast of South Carolina. There was little indication 12 hours earlier that cyclogenesis would commence in this area. One might argue that the inverted trough previously in the Gulf could have signaled the onset of cyclogenesis, if the trough had moved to the current position of the low with the 500mb flow. However, the 1800 GMT surface analysis (not shown) shows no indication of the trough translating northeastward across the Florida peninsula. Coinciding with the cyclonic development off the coast is a reorientation and strengthening of the 1000mb thermal gradient along the coast from Georgia to Maryland within the inner volume boundary. The presence of the coastal front and its contribution to the cyclone development is discussed by Bosart (1981). In addition, a significant thermal ridge has developed within the inner volume boundary.

The primary change in the 850mb contour pattern (Fig. 3b) is the southeastward extension of the trough over the

surface low. This trough now encompasses the entire northwest quadrant of the budget volume. Little change is seen in the 850mb isotherm pattern during the 12-hour period. The thermal patterns at the 1000 and 850mb levels indicate low-level destabilization within the inner volume boundary which would favor organized convection.

The 500mb wave (Fig. 3c) has moved eastward to Illinois and is more in phase with the thermal trough at this time. The wave is beginning to penetrate the northwest quadrant of the outer budget volume boundary. A weak ridge is seen in the isotherm pattern at this level throughout the inner volume boundary. The vorticity pattern (Fig. 7b) shows weak PVA over the northern half of the volume. Thermal advection, as depicted in the thickness pattern (Fig. 9b), is confined to the inner volume radius with warm advection to the east and weak cold advection to the west of the cyclone center.

The 1200 GMT 19 February surface pressure pattern (Fig. 4a) indicates significant cyclogenesis has occurred. The minimum pressure decreased by 9 mb in the 12-hour period ending at this time. The surface isobars show a highly symmetrical circular cyclone structure located entirely within

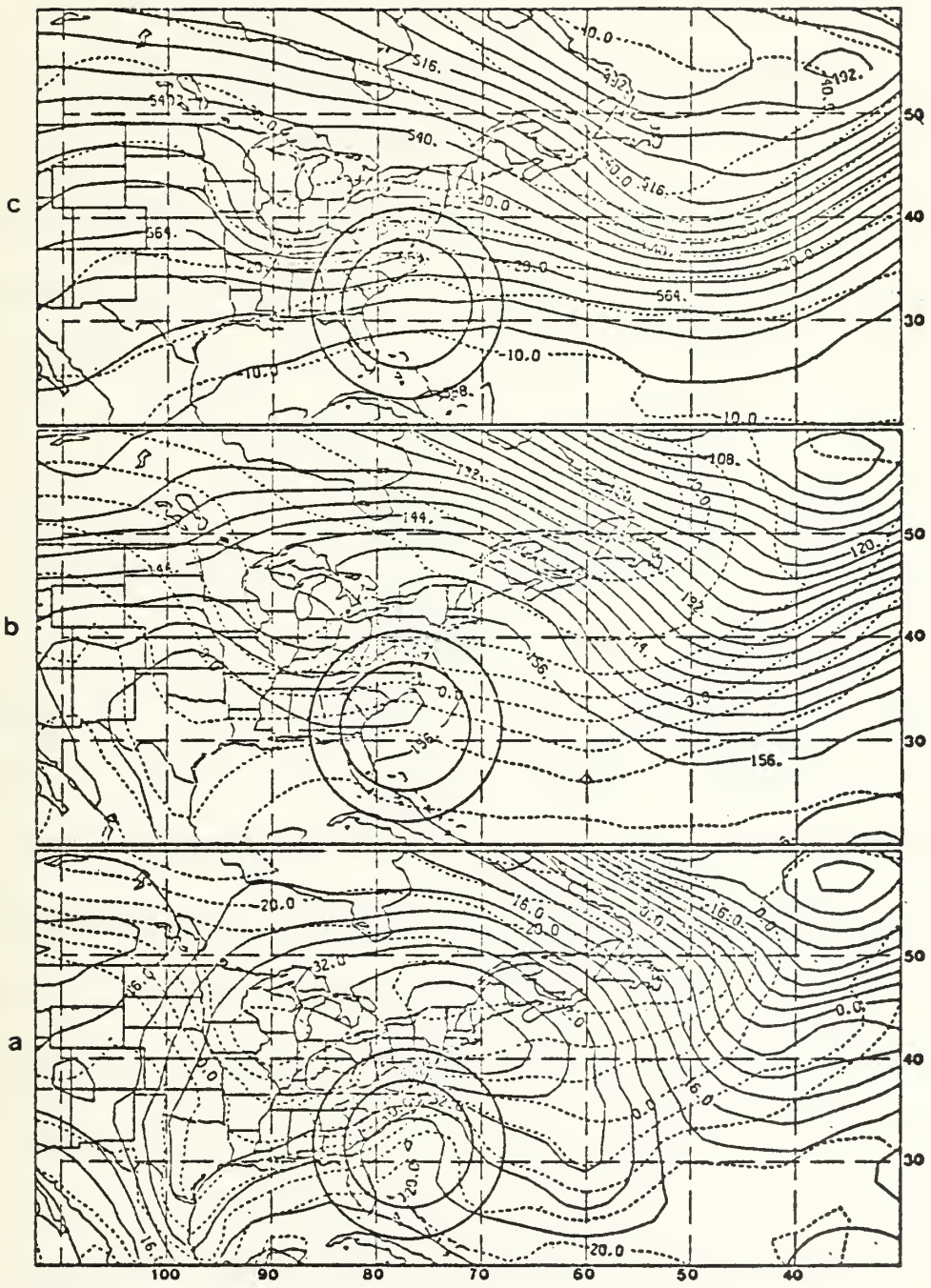

Figure 3. Same as Fig. 2 except for 0000 GMT 19 February 1979.

the inner budget radius. The 1000mb thermal ridge is considerably sharper and is in nearly perfect alignment with the cyclone center and associated pressure trough. The 1000mb isotherm pattern reveals the development of a baroclinic zone to the southwest of the cyclone within the inner budget volume. The 850mb height contours (Fig. 4b) now show closed cyclonic circulation centered in the northwest quadrant of the inner volume radius which indicates a northwest tilt of the cyclone axis toward the cold air. Significant changes in the 850mb isotherm pattern have occurred during this 12-hour period. The development of a thermal ridge over the surface center indicates that the warm core is penetrating to higher levels. This warming is likely the result of latent heat release through convection and the warm advection shown at the 850mb level 12 hours earlier.

The 500mb wave (Fig. 4c) is now centered over Pennsylvania and is nearly in phase with the thermal trough within the northwest quadrant of the outer budget volume boundary. The 500mb vorticity center (Fig. 7c) is now within the outer radius with significant PVA in the inner radius primarily to the northeast of the surface center. The thickness pattern (Fig. 9c) shows a warm ridge centered on the cyclone with

warm advection throughout the eastern half and cold advection throughout the western half of the outer budget radius.

Intense cyclogenesis continues during the next 12-hour period ending at 0000 GMT 20 February. During this period the surface pressure minimum (Fig. 5a) decreases by nearly 18 mb. At the same time, the cyclone takes a more easterly course following the maximum 500mb PVA region. The vertical structure indicates that the cyclone is nearing the mature stage. The circular surface and 850mb centers are nearly coincident and the isotherm patterns show a vertical alignment of the thermal ridge through the 850mb level (Fig. 5b). The 500mb wave (Fig. 5c) is almost directly over the surface cyclone and is encompassed by the outer budget radius. The thermal trough now lags the 500mb wave with an intensified thermal ridge within the eastern half of the outer volume boundary. Thus, the warm core now extends through the low troposphere. The thickness pattern (Fig. 10a) clearly illustrates a mature warm core structure. The vertical extension of the warm core through the 500mb level is most likely due to convection since little thermal advection is seen at this level prior to 0000 GMT. The mature structure indicates that little further deepening of the cyclone can

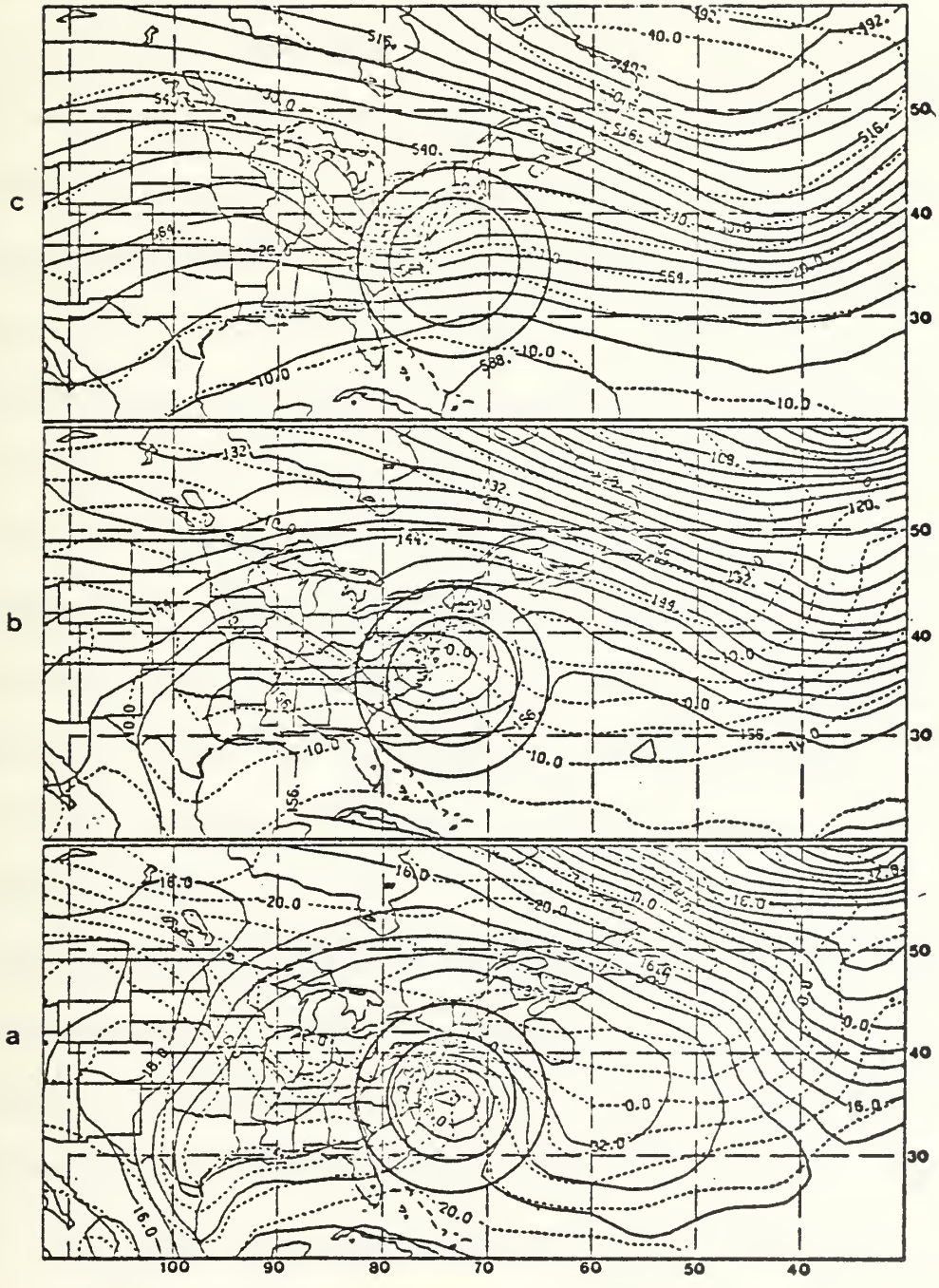

Figure 4. Same as Fig. 2 except for 1200 GMT 19 February 1979.

be expected. The 500mb vorticity pattern (Fig. 8a) shows PVA throughout the eastern half of the budget volume with maximum PVA due east of the cyclone center.

The surface pressure pattern (Fig. 6a) at 1200 GMT 20 February shows that the cyclone center has accelerated in an easterly direction during the previous 12 hours with little further deepening. The storm center moves nearly 250 nm eastward for an average velocity of approximately 20 knots. Little change is seen in the thermal structure through the low troposphere in the inner budget volume. This might indicate that a moist adiabatic lapse rate has been achieved by convection throughout much of the inner budget radius. The 500mb vorticity pattern (Fig. 9b) now shows moderate to strong PVA in the eastern half and definite negative vorticity advection (NVA) in the northwest quadrant of the outer volume boundary.

The intent of this synoptic overview has been to present the highlights of the development of the Presidents' Day Cyclone in terms of the mass and circulation fields as a prelude to the storm-following budget analyses in this thesis. The goal of budget studies of this storm is to quantify the forcing mechanisms of explosive maritime

cyclogenesis. A brief discussion of the quasi-Lagrangian technique employed in the budget study is presented in the next chapter.

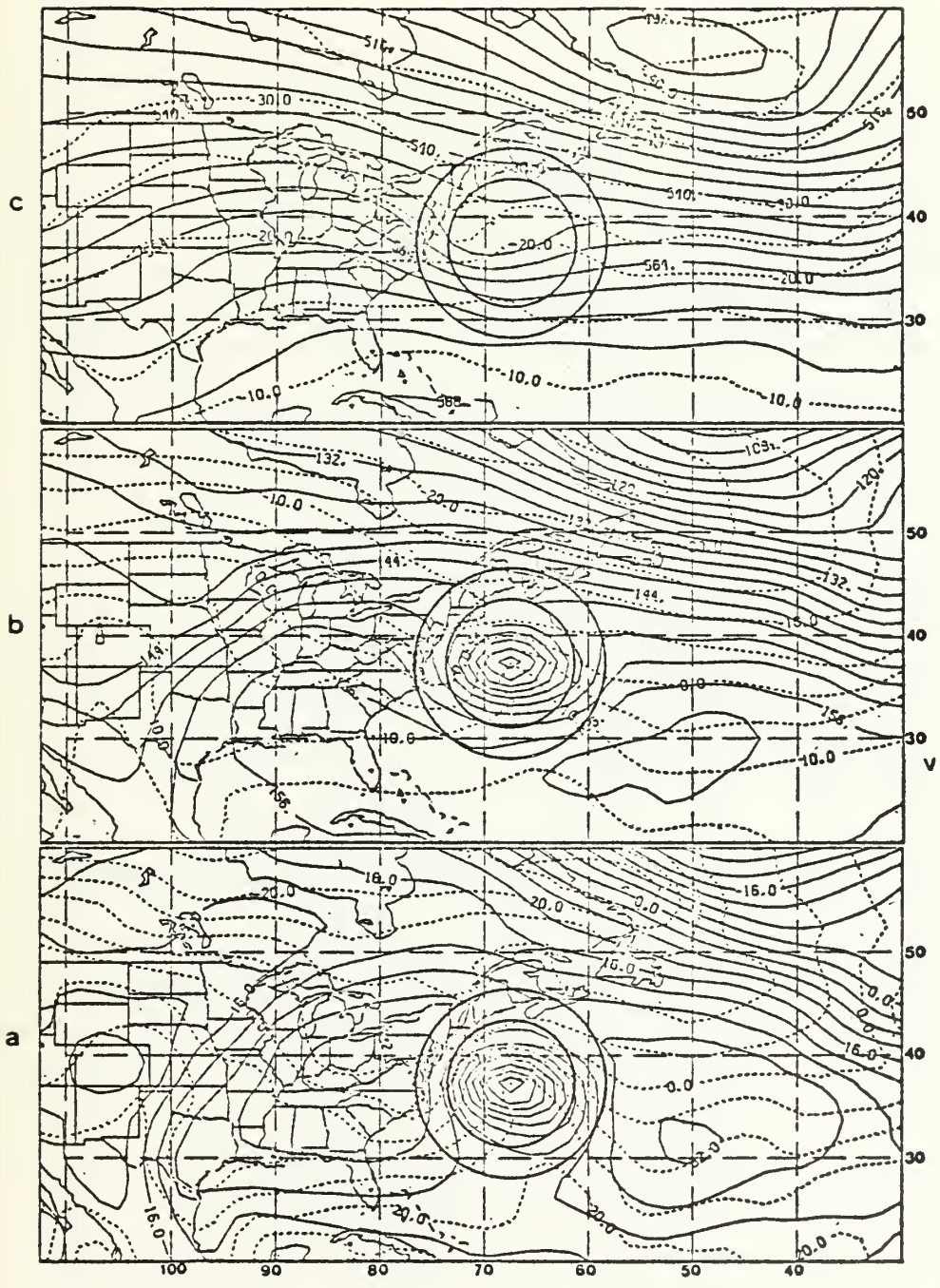

Figure 5. Same as Fig. 2 except for 0000 GMT 20 February 1979.

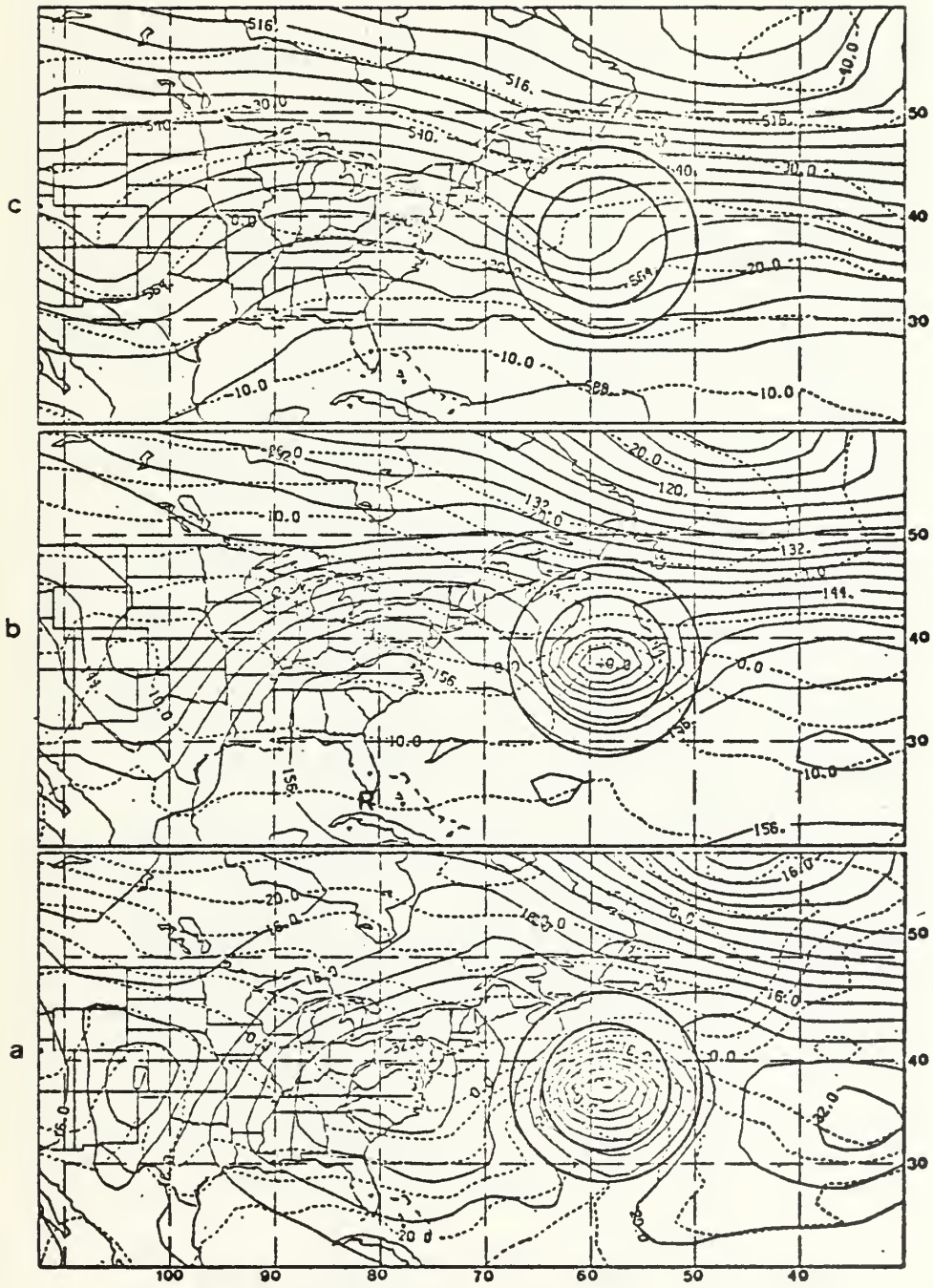

Figure 6. Same as Fig. 2 except for 1200 GMT 20 February 1979.

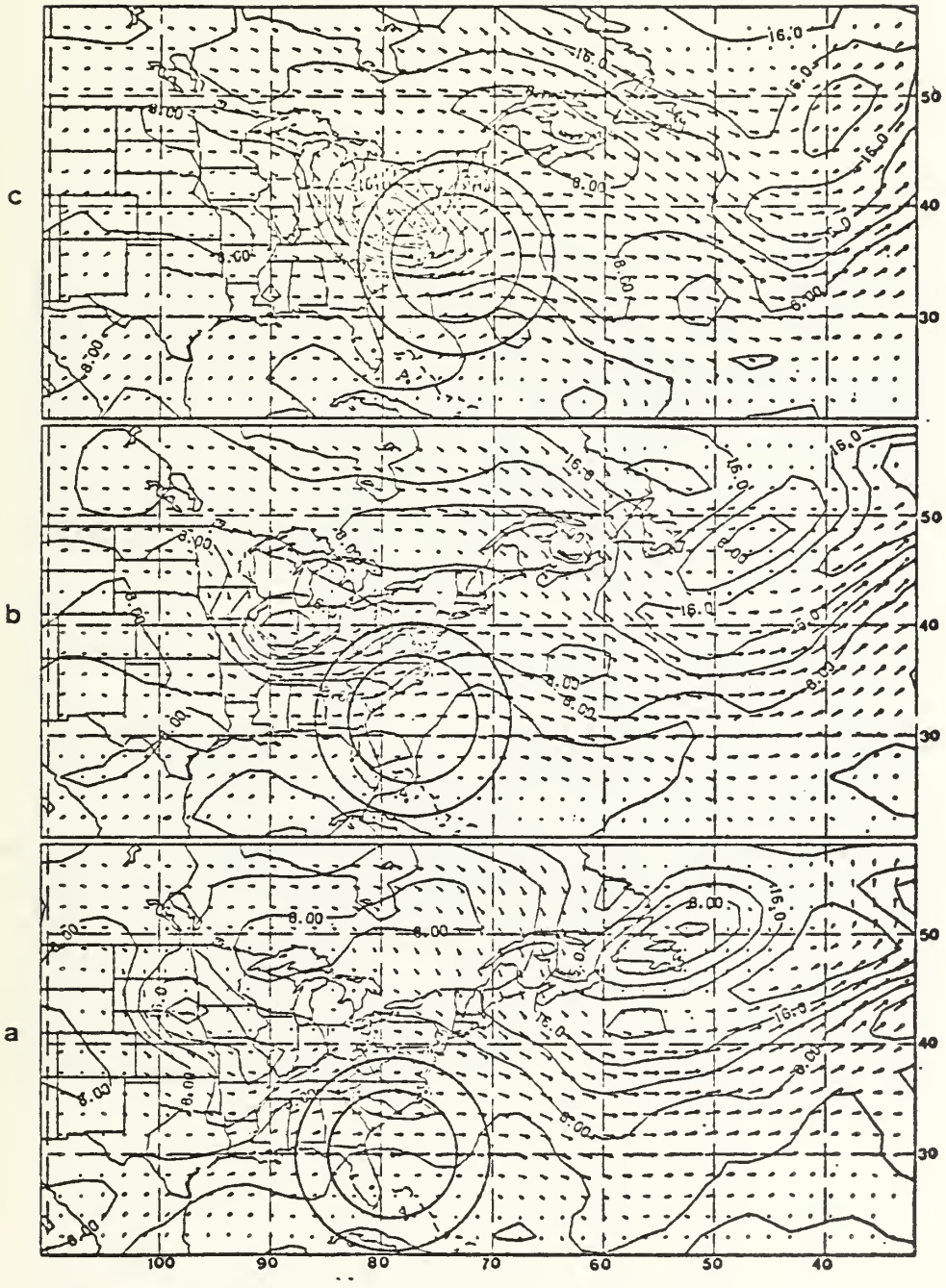

Figure 7. 500mb absolute vorticity fields (x 10^{-5} sec^{-1}) and wind vectors for a. 1200 GMT 18 February 1979, b. 0000 GMT 19 February 1979 and c. 1200 GMT 19 February 1979. Circles are 6 and 9 degree budget volume lateral boundaries.

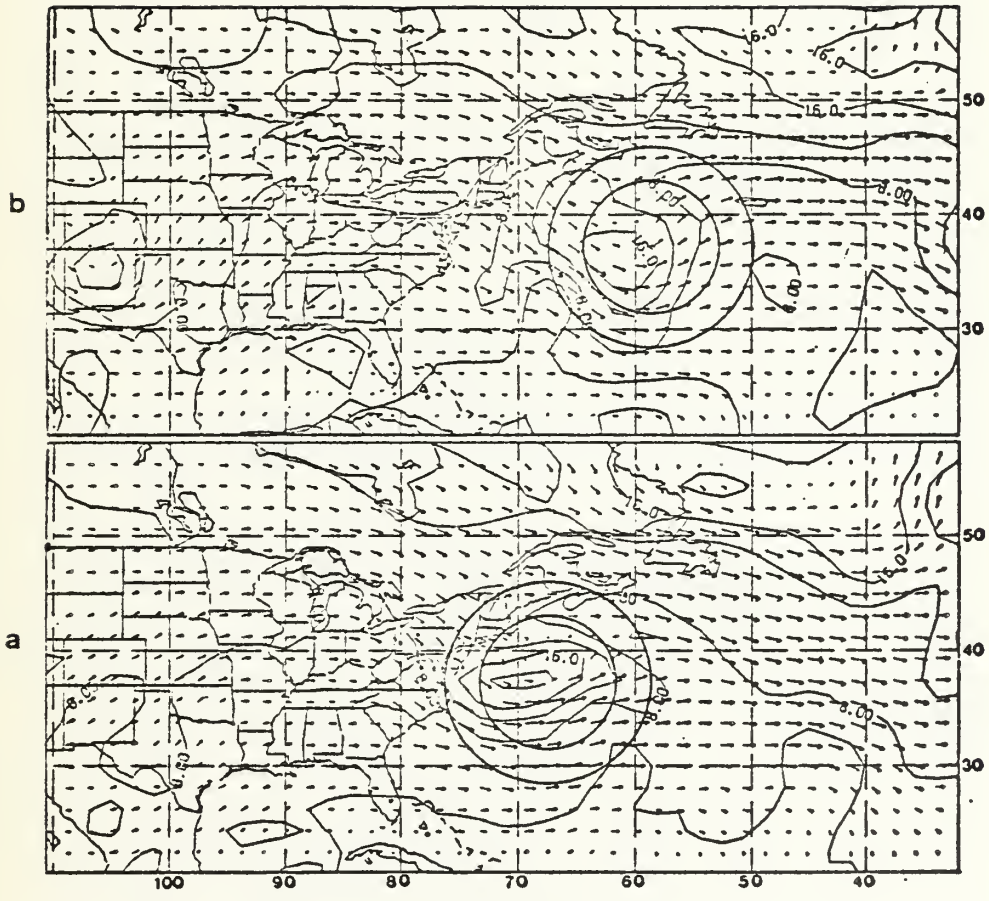

Figure 8. Same as Fig. 7 except for a. 0000 GMT 20 February 1979 and b. 1200 GMT 20 February 1979.

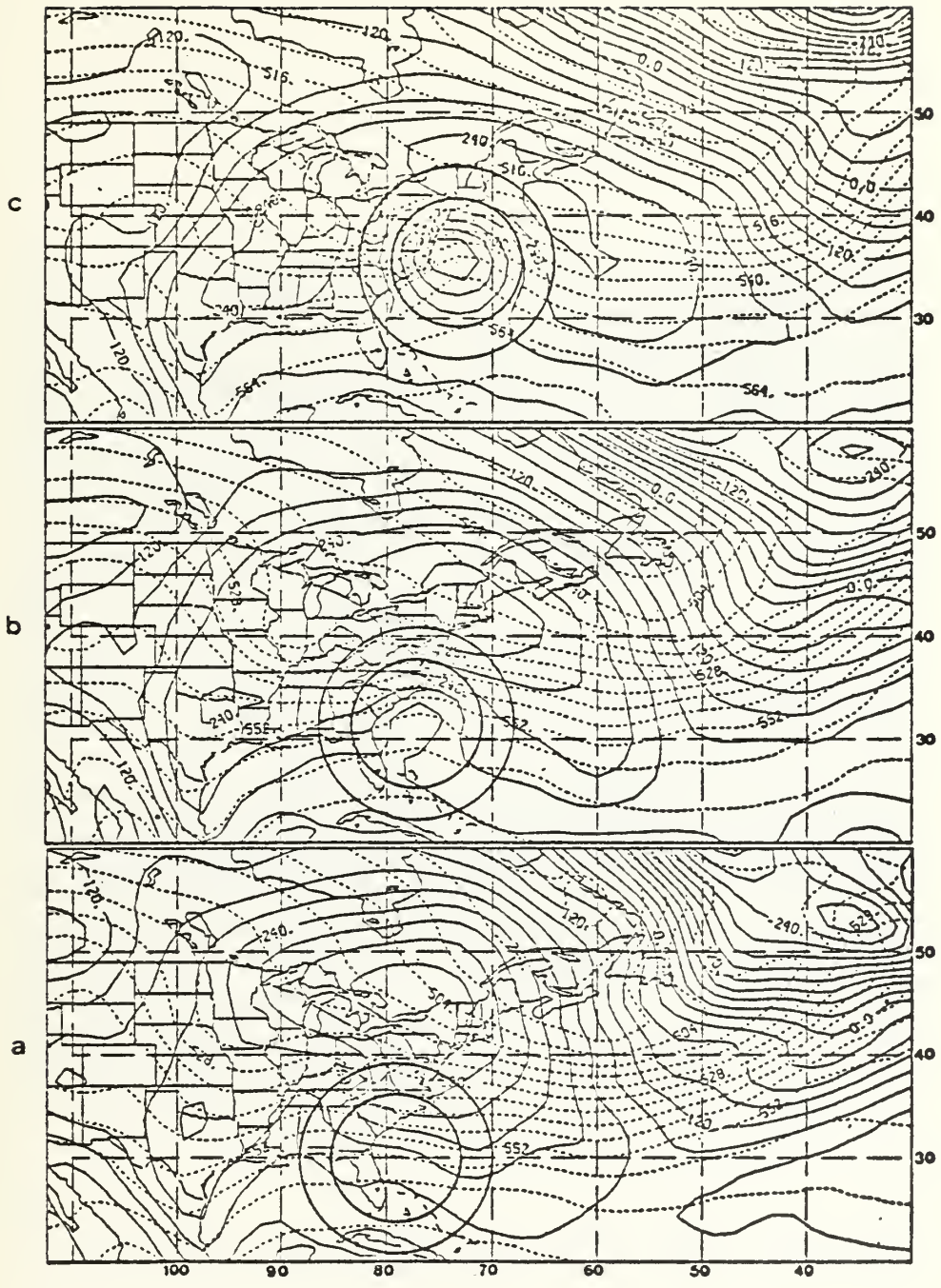

Figure 9. 1000-500mb thickness and 1000mb contour patterns for a. 1200 GMT 18 February 1979, b. 0000 GMT 19 February 1979 and c. 1200 GMT 19 February 1979. Thickness contours are dashed and labeled in decameters. 1000 mb contours are labeled in meters. Circles are 6 and 9 degree budget volume lateral boundaries.

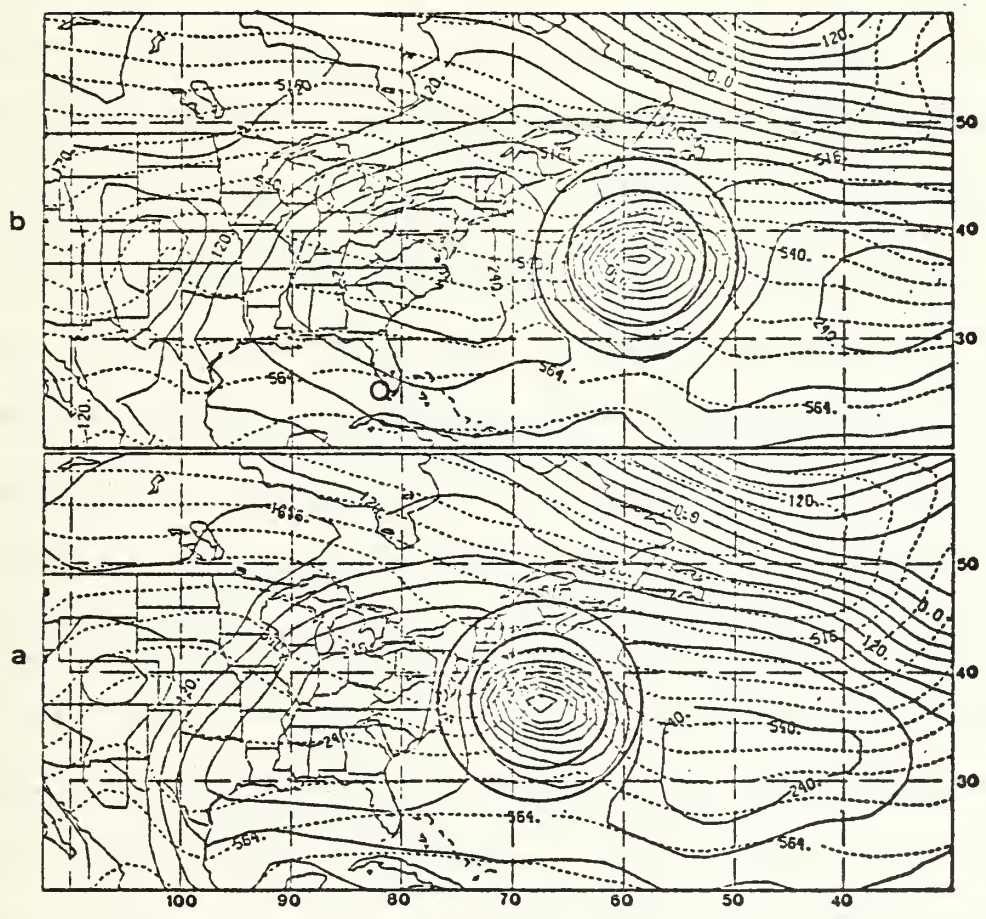

Figure 10. Same as Fig. 9 except a. 0000 GMT 20 February 1979 and b. 1200 GMT 20 February 1979.

III. QUASI-LAGRANGIAN DIAGNOSTIC TECHNIQUE

The objective of budget studies is to evaluate the changes of atmospheric properties within a specific atmospheric volume. Normally these studies have been used primarily to study the general circulation and planetary scale balances of atmospheric properties such as mass, momentum and kinetic energy. For synoptic-scale studies the approach has been to evaluate changes in these properties within a stationary volume (Kung and Baker, 1975; Smith, 1973). The effects of synoptic-scale disturbances migrating through the volume are quantitatively evaluated relative to the fixed volume only. This approach is not well suited to the study of cyclone development since changes in the budget volume can be due to the movement of the cyclonic circulation into or out of the volume as well as due to cyclone development.

The QLD budget approach employed in this thesis uses a budget volume which translates with the cyclone. This method permits a quantitative evaluation of the changes in the budget property relative to the cyclone. Specifically, this system isolates the horizontal advection and transport relative to the cyclone from the horizontal advection and transport associated with the translation of the cyclone.

Further, the vertical redistribution of the budget property is the result of the vertical transport processes in the vicinity of the cyclone. Thus, the QLD technique is well suited to the study of cyclogenesis. Table II presents an updated list of recently completed studies employing the QLD method.

TABLE II

PREVIOUS QUASI-LAGRANGIAN DIAGNOSTIC BUDGET STUDIES

(EXTRACTED IN PART FROM WASH, 1978)

Property	Researcher(s)
Available Potential Energy	Spaete 1974
Circulation	Wash 1975
Mass	Johnson and Downey 1976
Absolute Angular Momentum	Johnson and Downey 1976
Kinetic Energy	Chen and Bosart 1977
Absolute Angular Momentum	Wash 1978
Mass	Roman 1981
Mass	Tallman 1982

The budget equation is evaluated with respect to a budget volume in spherical coordinates (Appendix B). In this thesis, the budget volume is centered over and maintains its position relative to the surface pressure minimum

of the Presidents' Day Cyclone. The volume is defined in the vertical by 10 mandatory pressure levels (1000, 850, 700, 500, 400, 300, 250, 200, 150 and 100 mbs) and horizontally by radii for example, six degrees of latitude. Appendix B establishes the quasi-Lagrangian budget volume coordinate system and the generalized budget equations that can be applied to any selected atmospheric property.

The first step in the calculation of the budgets is to interpolate the u and v wind component values at the rectangular gridpoints in the FGGE data set to the budget volume gridpoints. The interpolated winds are then converted to normal and tangential components relative to the circular budget volume boundaries. Additionally, the movement of the budget volume ($\underset{\sim}{W}_o$) is used to compute the normal and tangential components relative to the translating volume.

The budget equations for the circulation and angular momentum budgets in pressure coordinates are presented in Tables III and IV. In the vorticity budget formulation, the horizontal advection and divergence terms are combined to form the lateral transport using the Gauss Divergence Theorem,

$$\int_A \int -(\underset{\sim}{U}-\underset{\sim}{W})\cdot\nabla\zeta_a - \zeta_a \nabla\cdot(\underset{\sim}{U}-\underset{\sim}{W})\, dA$$

$$= -\int_A \int \nabla\cdot\zeta_a(\underset{\sim}{U}-\underset{\sim}{W})\, dA = -\int \zeta_a(\underset{\sim}{U}-\underset{\sim}{W})_\beta\, dL.$$

The vertical redistribution occurs through the vertical advection term and the friction and tilting terms complete the budget. The angular momentum budget is formulated by combining the continuity and angular momentum equations. Since there is no divergence term, the vertical redistribution occurs through a vertical transport term. The friction term completes this budget.

The budget volume grid consists of 36 equally spaced points around each circular lateral boundary at each pressure level. Absolute vorticity and angular momentum values are computed at each of the volume gridpoints. The calculations of the time tendency, transport and source/sink terms are based on these gridpoint values. The tilting term in the vorticity equation is computed as a source. There are no sources of absolute angular momentum within the budget volume, and the only sink is due to friction which is computed using a stability independent parameterization scheme (Johnson and Downey, 1976) with a constant geostrophic drag coefficient (0.035).

The transport terms are broken into mean and eddy modes (Table V). The purpose of this statistical partitioning

is to isolate changes in the budget property associated with the synoptic-scale mean and eddy circulations. The mean and eddy modes represent the transport by the irrotational and rotational wind components, respectively. In this context, the mean and eddy modes are analogous to the divergence and horizontal advection terms in the vorticity equation. In this study the divergence and advection terms are calculated for comparison with the mean and eddy modes. The comparisons serve to further substantiate the validity of the mean and eddy mode partitioning in the QLD technique.

The FGGE vertical velocity fields were calculated based on divergences derived through a nonlinear normal mode initialization scheme. An objective of this thesis is to compare the FGGE vertical velocities with the vertical velocity values derived via the QLD method in the mass budget of the Presidents' Day Cyclone (Roman, 1981). The purpose of this comparison is to aid in the assessment of the vertical velocities computed in the budget technique. The comparison is presented in conjunction with the analysis of the budget vertical transport term in the next chapter.

TABLE III

QUASI-LAGRANGIAN CIRCULATION BUDGET EQUATION IN ISOBARIC VERTICAL COORDINATES

(after Wash, 1978)

$$C_a = \int_{1000mb}^{100mb} \int_0^{\beta} \int_0^{2\pi} \frac{1}{g} \zeta_a r^2 \sin\beta \, d\alpha d\beta (-dp)$$

where C_a is absolute circulation and ζ_a is absolute vorticity.

The budget equation is

$$\frac{\delta C}{\delta t} a = LT(C_a) + VT(C_a) + S(C_a)$$

where the lateral transport is

$$LT(C_a) = \int_{1000mb}^{100mb} \int_0^{2\pi} \frac{1}{g} (\underset{\sim}{U} - \underset{\sim}{W})_\beta \zeta_a r \sin\beta \, d\alpha (-dp) \Big|_\beta$$

and the vertical advection is

$$VT(C_a) = \int_0^{\beta} \int_0^{2\pi} \frac{1}{g} \omega \frac{\partial \zeta}{\partial p} a \; r^2 \sin\beta \, d\alpha d\beta.$$

The source/sink term is

$$S(C_a) = \int_{1000mb}^{100mb} \int_0^{\beta} \int_0^{2\pi} \frac{1}{g} \frac{d\zeta}{dt} a \; r^2 \sin\beta \, d\alpha d\beta (-dp).$$

See Appendix B for notation explanation.

TABLE IV

QUASI-LAGRANGIAN ANGULAR MOMENTUM BUDGET EQUATION IN ISOBARIC VERTICAL COORDINATES

(after Wash, 1978)

$$G_a = \int_{1000mb}^{100mb} \int_0^{\beta} \int_0^{2\pi} \frac{1}{g} g_a r^2 \sin\beta \, d\alpha d\beta (-dp)$$

where G_a is the volume integral of absolute angular momentum g_a.

The budget equation is

$$\frac{\delta G}{\delta t}a = LT(G_a) + VT(G_a) + S(G_a)$$

where the lateral transport is

$$LT(G_a) = \int_{1000mb}^{100mb} \int_0^{2\pi} \frac{1}{g} (\underset{\sim}{U}-\underset{\sim}{W})_{\beta} g_a r \sin\beta \, d\alpha (-dp) \Big|_{\beta}$$

and the vertical divergence of the vertical transport is

$$VT(G_a) = \int_{1000mb}^{100mb} \int_0^{\beta} \int_0^{2\pi} \frac{1\partial}{g\partial p} (\omega g_a) r^2 \sin\beta \, d\alpha d\beta (-dp).$$

The sink term is

$$S(G_a) = \int_{1000mb}^{100mb} \int_0^{\beta} \int_0^{2\pi} \frac{1}{g} \frac{dq}{dt}a \, r^2 \sin\beta \, d\alpha d\beta (-dp).$$

See Appendix B for notation explanation.

TABLE V

PARTITION OF LATERAL TRANSPORT INTO MEAN AND EDDY MODES

(after Wash, 1978)

$$EM(C_a) = \int_{1000mb}^{100mb} \int_0^{2\pi} \frac{1}{g} \overline{\zeta_a^* (\underset{\sim}{U}-\underset{\sim}{W})_\beta^*} \, r\sin\beta \, d\alpha(-dp)\Big|_\beta$$

$$MM(C_a) = \int_{1000mb}^{100mb} \int_0^{2\pi} \frac{1}{g} \bar{\zeta}_a^\alpha \overline{(\underset{\sim}{U}-\underset{\sim}{W})_\beta^\alpha} \, r\sin\beta \, d\alpha(-dp)\Big|_\beta$$

$$EM(G_a) = \int_{1000mb}^{100mb} \int_0^{2\pi} \frac{1}{g} \overline{g_a^* (\underset{\sim}{U}-\underset{\sim}{W})_\beta^*} \, r\sin\beta \, d\alpha(-dp)\Big|_\beta$$

$$MM(G_a) = \int_{1000mb}^{100mb} \int_0^{2\pi} \frac{1}{g} \bar{g}_a^\alpha \overline{(\underset{\sim}{U}-\underset{\sim}{W})_\beta^\alpha} \, r\sin\beta \, d\alpha(-dp)\Big|_\beta$$

EM is the eddy mode and MM is the mean mode.

Note that $(\bar{\ })^\alpha = \frac{1}{2\pi} \int_0^{2\pi} (\ ) \, d\alpha$

and $(\ )^* = (\ ) - (\bar{\ })^\alpha$ is the deviation of

the property from its mean around a lateral boundary. See Tables III and IV and Appendix B for notation explanation.

IV. QUASI-LAGRANGIAN BUDGET ANALYSIS

A. GENERAL

The absolute circulation or vorticity and absolute angular momentum budget results are presented in this chapter. Emphasis is placed on the vorticity budget since the results are similar and vorticity analyses are more commonly used to describe cyclone development. The angular momentum results are discussed in depth where significant differences exist, particularly in the vertical transport term.

The results are presented by means of layer or level/time or time period cross-sections and selected vertical profiles. Results are presented for two radii, 6° and 9°, which were illustrated in the synoptic discussion. Values are displayed on levels or layers over 6-hour time periods. For example, the 600mb layer extends from 700 to 500mb and the 1500 GMT time period runs from 1200 to 1800 GMT. The sign convention is positive for processes which produce a vorticity or angular momentum increase such as inward transport, inward horizontal advection and sources. Upward vertical velocity (omega) is negative (pressure coordinates).

B. TIME TENDENCY

The dramatic buildup of absolute vorticity within the budget volume during the development of the Presidents' Day Cyclone is illustrated by the vorticity time sections in Fig. 11. These patterns reflect the vorticity maximum developing within the budget radii at the 1000 mb level (Fig. 12) and the vorticity maxima moving into the budget circles at the 500 and 300 mb levels (Figs. 7 and 13 respectively).

The vorticity time section patterns (Fig. 11) within both radii are similar with minima occurring in the 225mb layer during the 1500 GMT 18 February time period. These minima are seen in terms of anticyclonic shear and curvature within the budget radii in the 300mb wind field (Fig. 14a). The vorticity values are greater in the 6° radius than those in the 9° radius after the 0900 GMT 19 February period. The larger gradient with respect to time in the inner radius depicts the rapid increase and concentration of cyclonic circulation as the storm develops. Maxima in both volumes occur in the upper layers during the 0900 GMT 20 February period. The larger vorticity increase with time in the upper layers is due to the development of cyclonic shear and

curvature as the upper tropospheric trough and associated jet maximum dominate the southern half of the inner budget volume (Fig. 14b). The vorticity profiles (Fig. 15) at the beginning and end of the intense cyclogenesis period show that the largest increase occurs in the upper layers.

Vorticity time tendencies computed over 6-hour intervals are depicted in Fig. 16. These patterns show positive tendencies in all layers and time periods with the exception of the lower layers within the inner radius during the final time period. Both patterns show primary and secondary maxima. The primary maximum in the 9° radius (350mb layer, 0300 GMT 19 February period) occurs earlier than the corresponding maximum in the 6° radius. The outer region of the cyclone is spinning-up earlier in response to the influence of the upper level trough and jet maximum at this time. As the trough overtakes the lower level cyclone, the 6° radius shows a large vorticity increase. The secondary maxima occur during the same period (2100 GMT 19 February) in each volume, but at a higher layer. These maxima are associated with the strong cyclonic shear and curvature north of the upper level jet core which is located within the budget volume at this time (Fig. 14b). The magnitude of the secondary

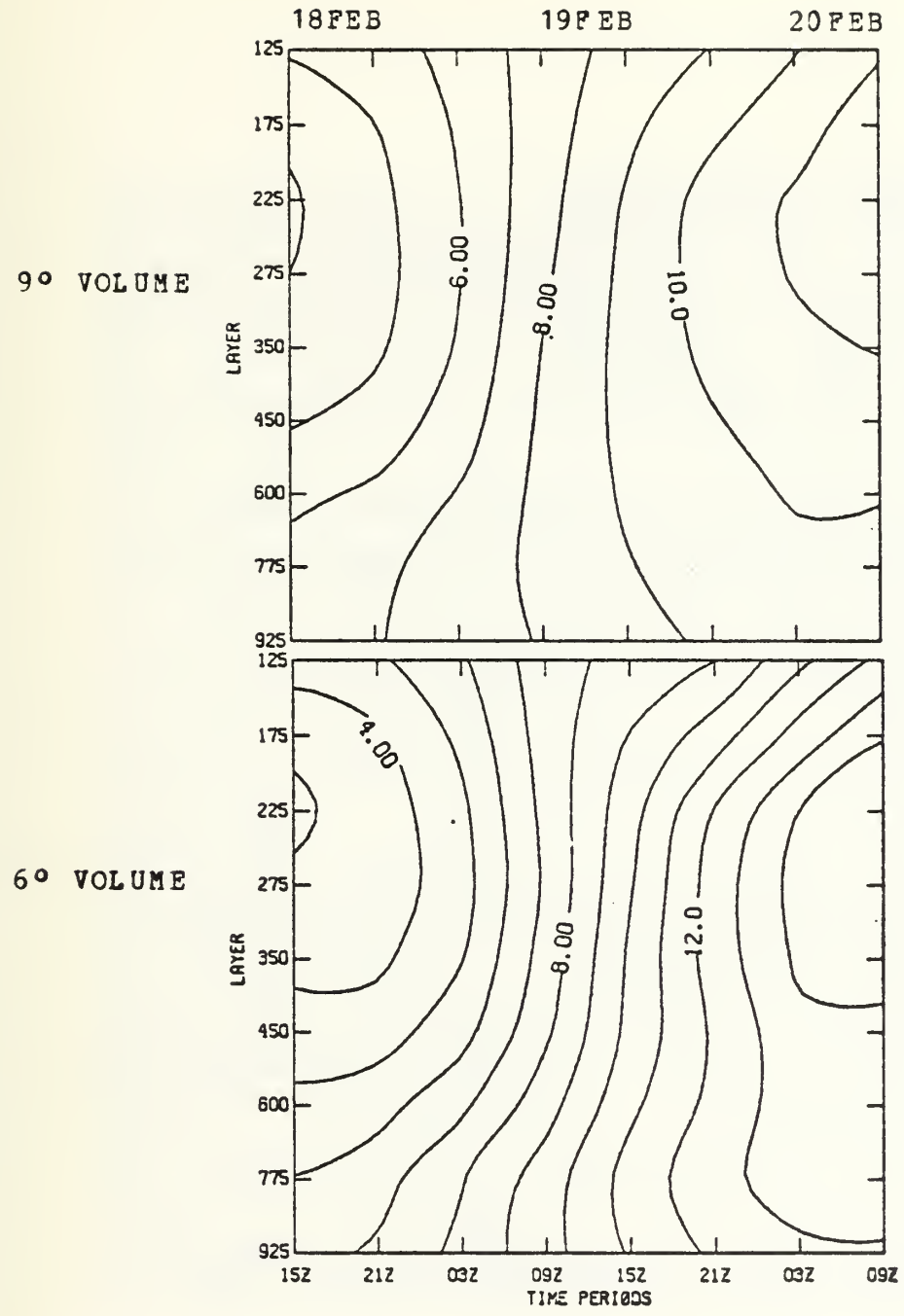

Figure 11. Absolute vorticity time sections (x 10^{-5} sec^{-1}).

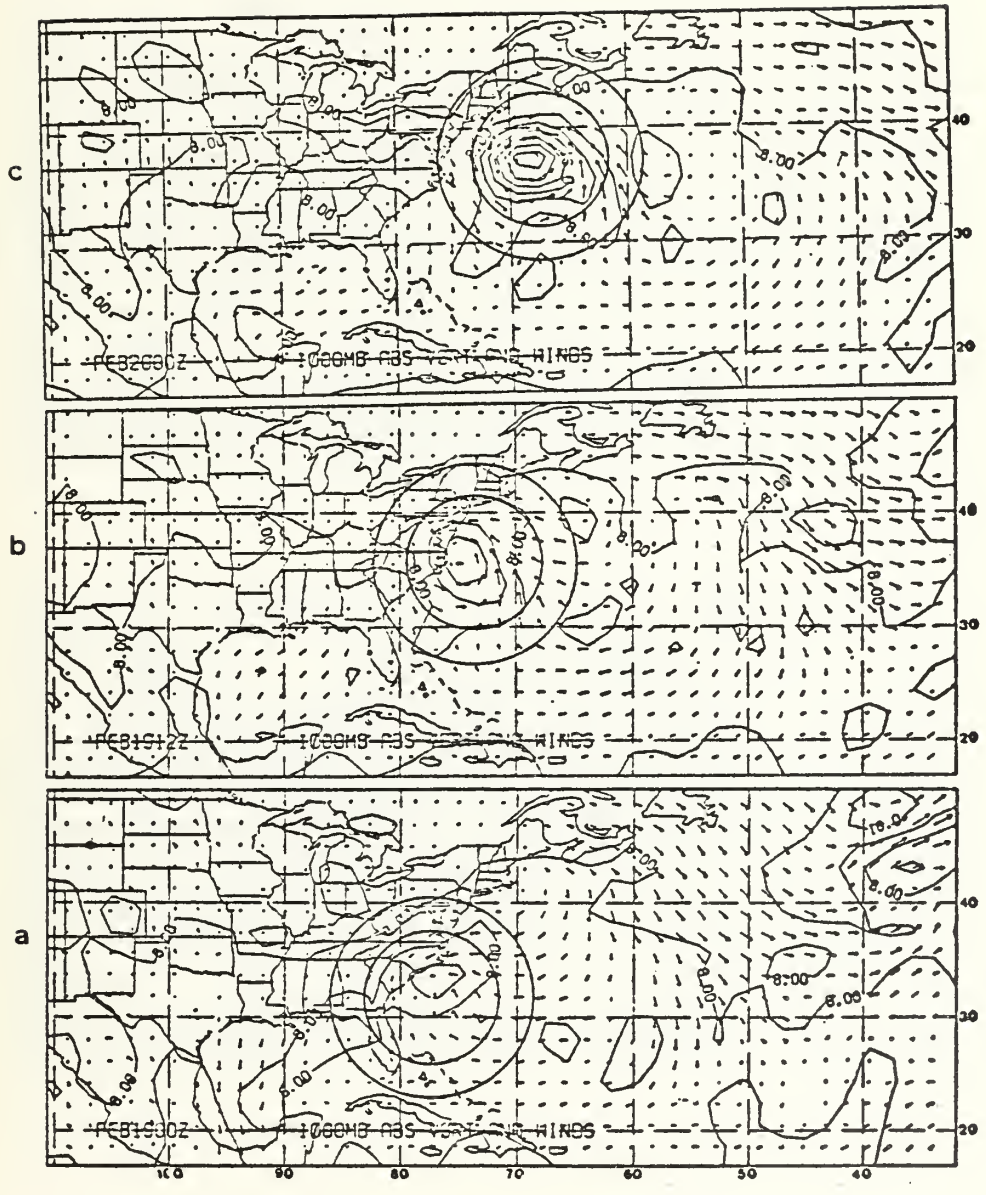

Figure 12. 1000mb wind vectors and absolute vorticity (x 10^{-5} sec^{-1}) for a. 0000 GMT 19 February 1979, b. 1200 GMT 19 February 1979 and c. 0000 GMT 20 February 1979. Circles are 6 and 9 degree budget volume lateral boundaries.

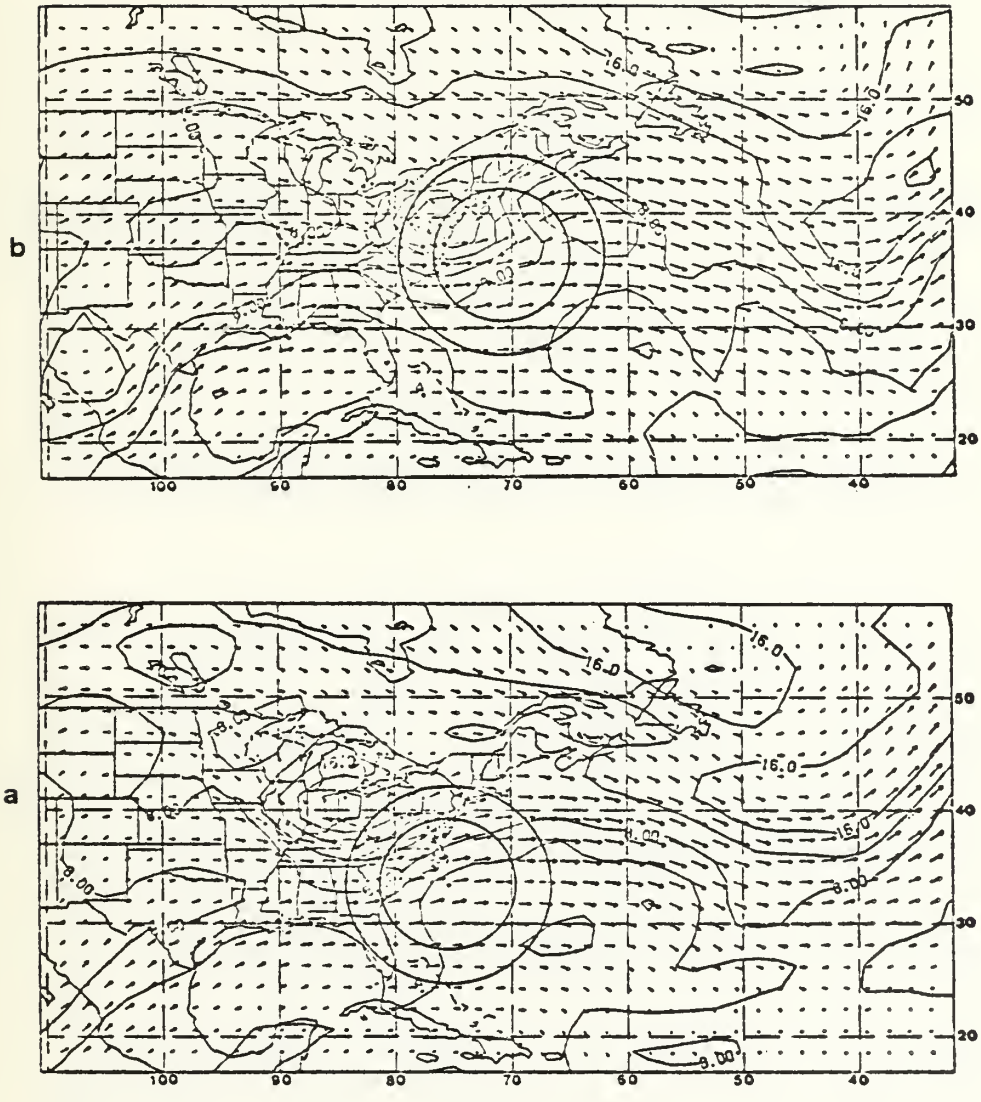

Figure 13. 300 mb wind vectors and and absolute vorticity (x 10^{-5} sec^{-1}) for a. 0600 GMT 19 February and b. 1800 GMT 19 February 1979. Circles are 6 and 9 degree budget volume lateral boundaries.

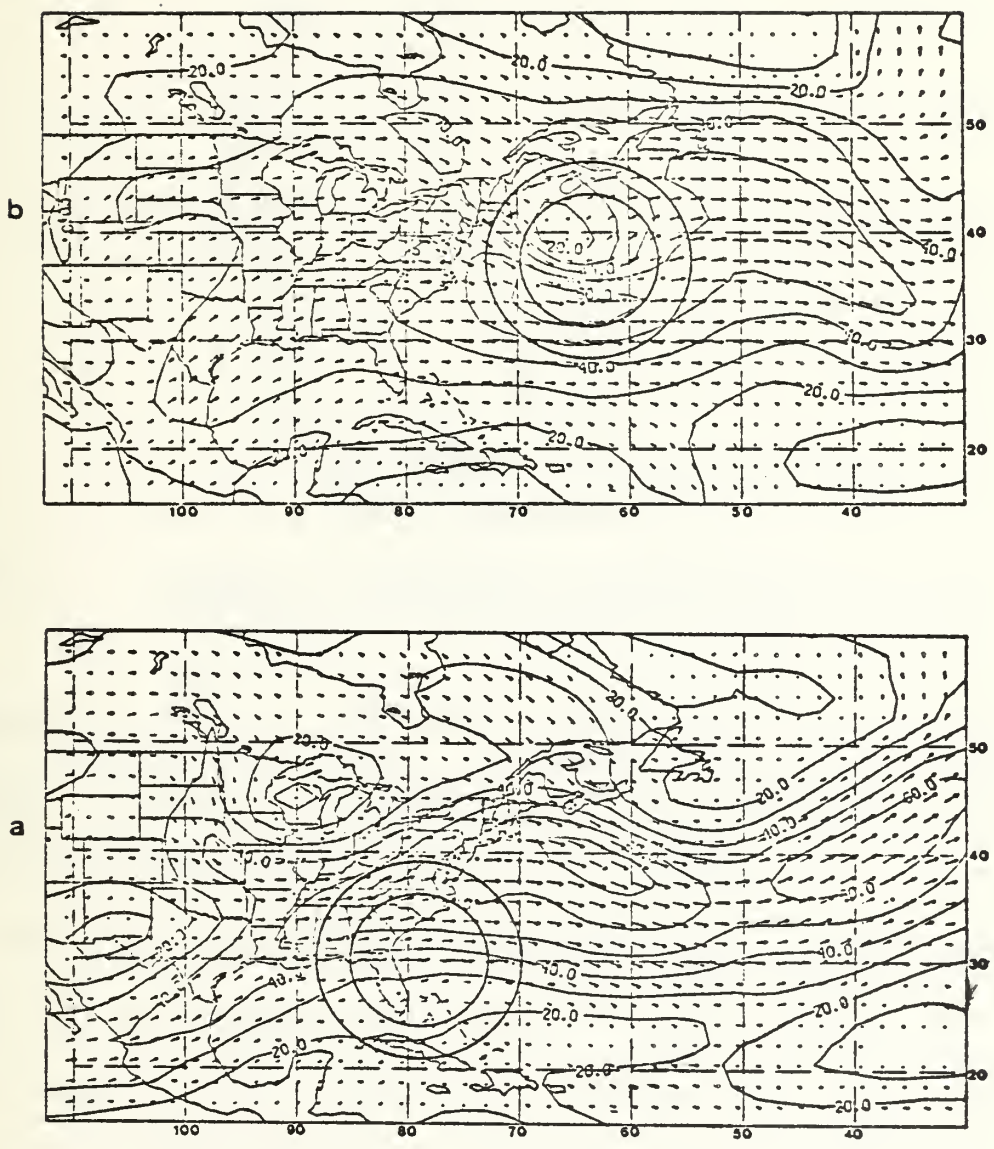

Figure 14. 300 mb wind vectors and isotachs (m sec^{-1}) for a. 1800 GMT 18 February and b. 0600 GMT 20 February 1979. Circles are 6 and 9 degree budget volume lateral boundaries.

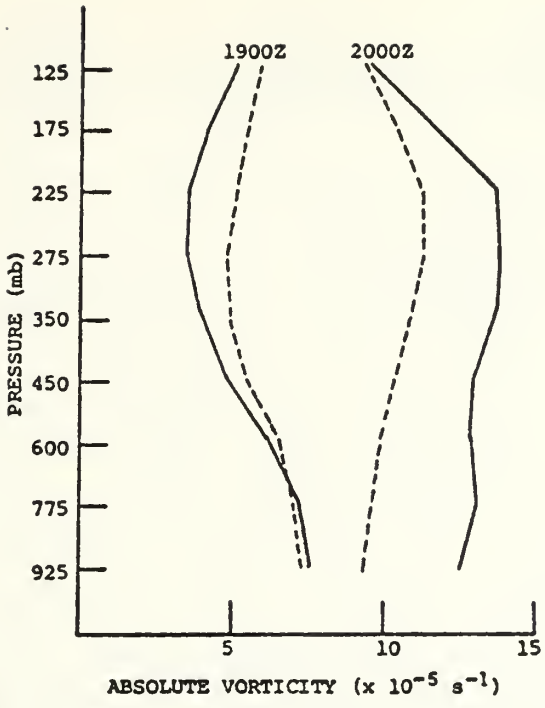

Figure 15. Absolute vorticity profiles for radius six (solid) and radius nine (dashed).

maximum in the 6° radius is nearly twice that in the 9° radius, because the maximum cyclonic curvature and shear vorticity occur within the inner boundary.

The absolute angular momentum time section patterns (Fig. 17) are similar to those of absolute vorticity, except the values in the outer radius exceed those in the inner radius. This difference is because storm angular momentum, $g_a = \underset{\sim}{k} \cdot \underset{\sim}{R} \times (\underset{\sim}{U}-\underset{\sim}{W})_\beta$, is proportional to the distance (R) from the storm center. The absolute angular momentum (Fig. 18)

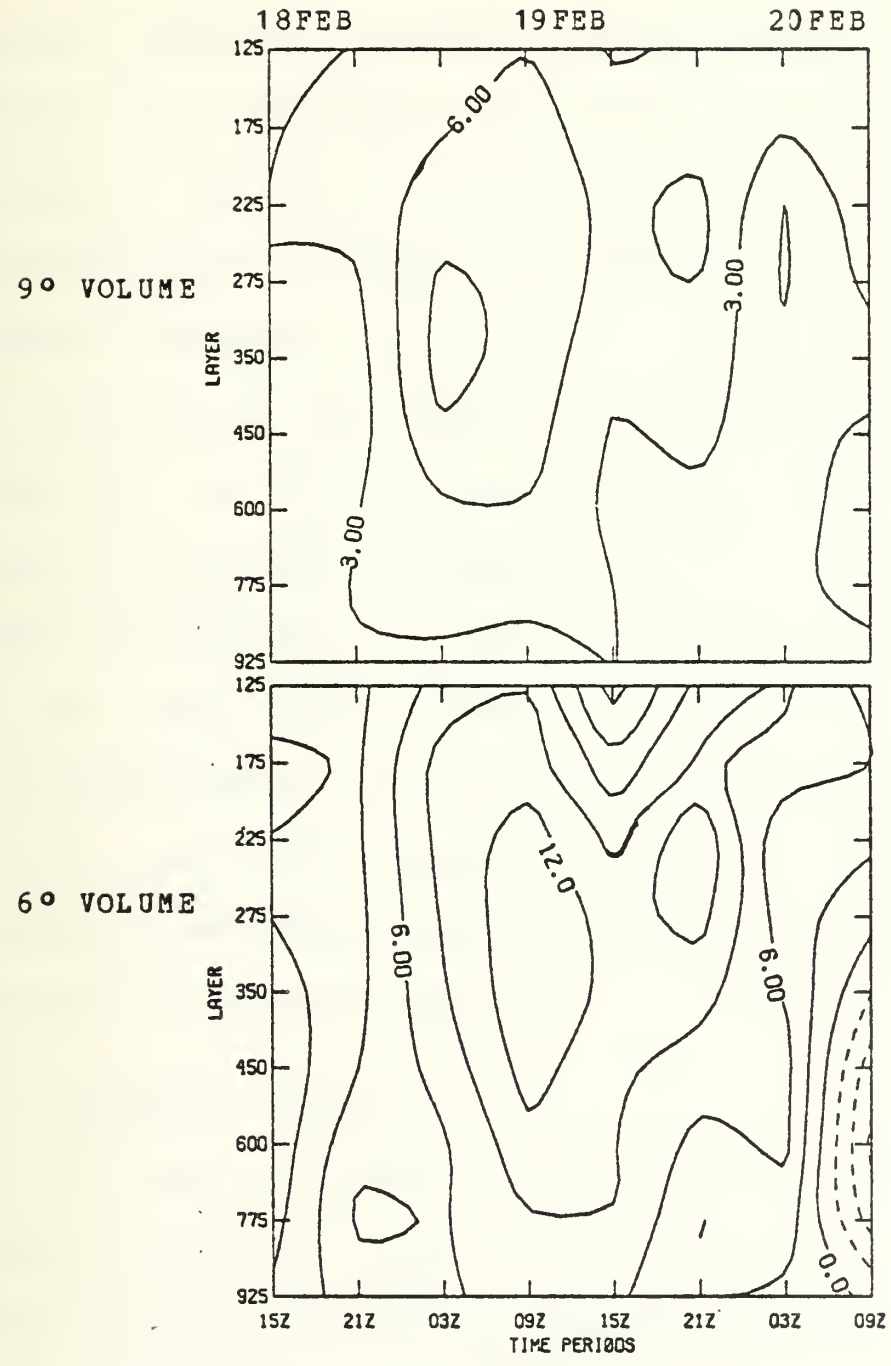

Figure 16. Absolute vorticity time tendencies over 6 hours (x 10^{-10} sec^{-2}). Dashed indicates negative values.

and vorticity time tendency patterns exhibit remarkable similarities with virtually coincident maxima. The larger angular momentum tendencies in the larger volume again reflect the dependence of this property on radius. The buildup of angular momentum within the budget volume portrayed in these patterns is consistent with the findings of Johnson and Downey (1976).

In summary, the vorticity and angular momentum patterns show that the largest increases occur within the 24-hour period of intense cyclogenesis (0000 GMT 19 February through 0000 GMT 20 February). The maximum vorticity buildup occurs in the upper layers because the polar jet core moves into the budget volume. The primary difference between the vorticity and angular momentum buildup is that the maximum angular momentum is found at a lower layer particularly in the 6° radius volume (Fig. 17).

C. LATERAL TRANSPORT

The lateral transport of absolute vorticity (Fig. 19) is the most important forcing term in the budget. The maximum inward transport occurs in the upper layers, although the transport is positive for nearly all of the layers. The maximum in the smaller volume occurs later, is in a lower

layer and is considerably greater in magnitude than the maximum in the larger volume. Both maxima occur within the 24-hour period of intense cyclogenesis; in particular, the larger maximum in the inner volume occurs during the period of most rapid deepening (1200-1800 GMT 19 February). The maximum transport in the larger volume occurs earlier (0600 GMT 19 February) as the vorticity maximum approaches the northwestern portion of the outer boundary (Fig. 13a). Twelve hours later, the vorticity maximum crosses the 6° boundary (Fig. 13b) and produces the larger maximum transport at the inner radius.

As described in the preceding chapter, the total lateral transport can be partitioned into mean and eddy mode components. The purpose of this partitioning is to break the total transport into components to improve the interpretation of the lateral transport dynamic forcing. The mean mode represents the mean vorticity transport by the average normal wind component (mean divergence or convergence), while the eddy mode is the transport due to the covariance of the vorticity and normal wind component deviations. In more general terms, the mean mode transport is due to the mean inflow and outflow of the cyclone and the eddy mode

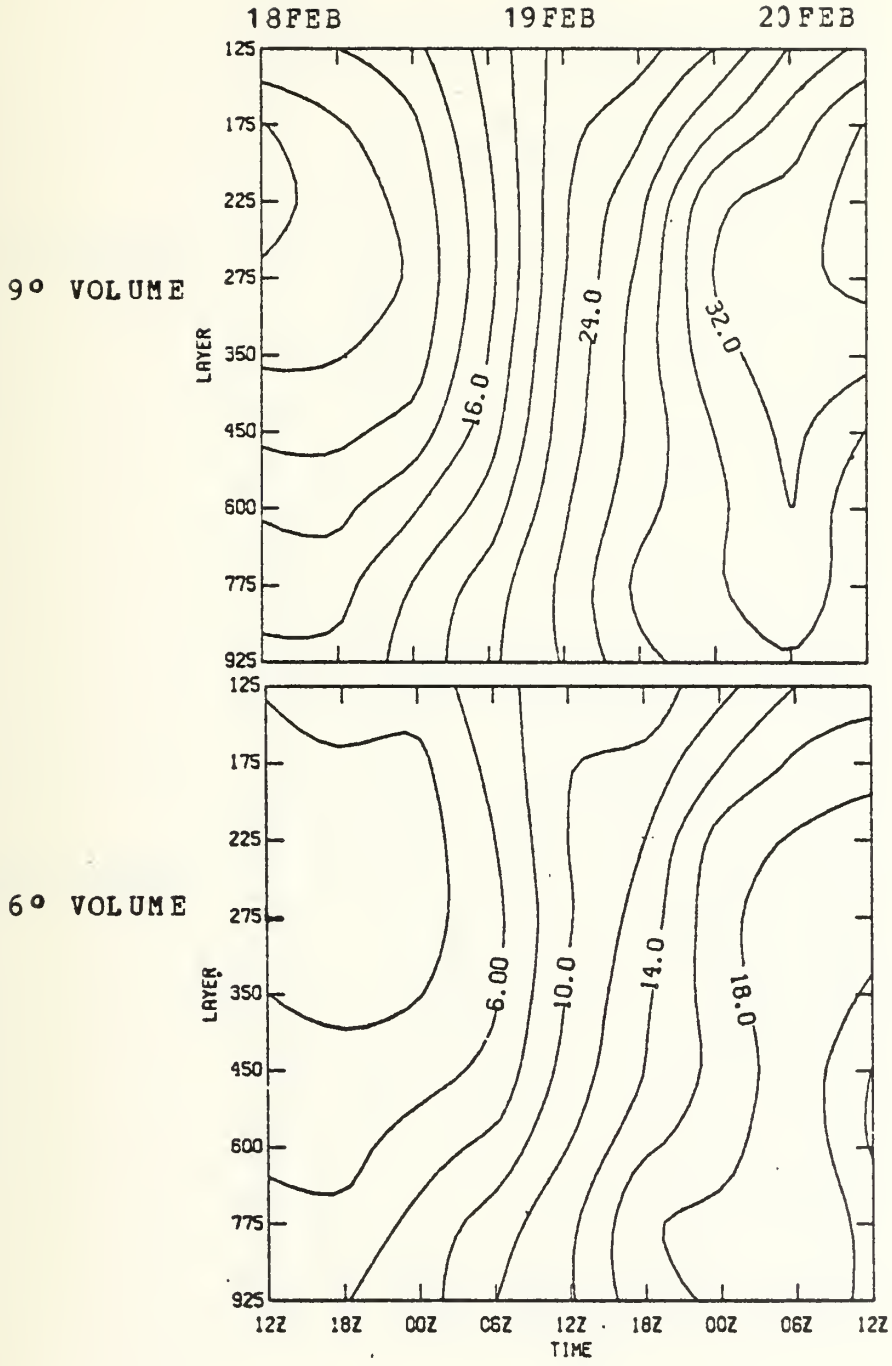

Figure 17. Absolute angular momentum time sections (x 10^{10} cm sec^{-2}).

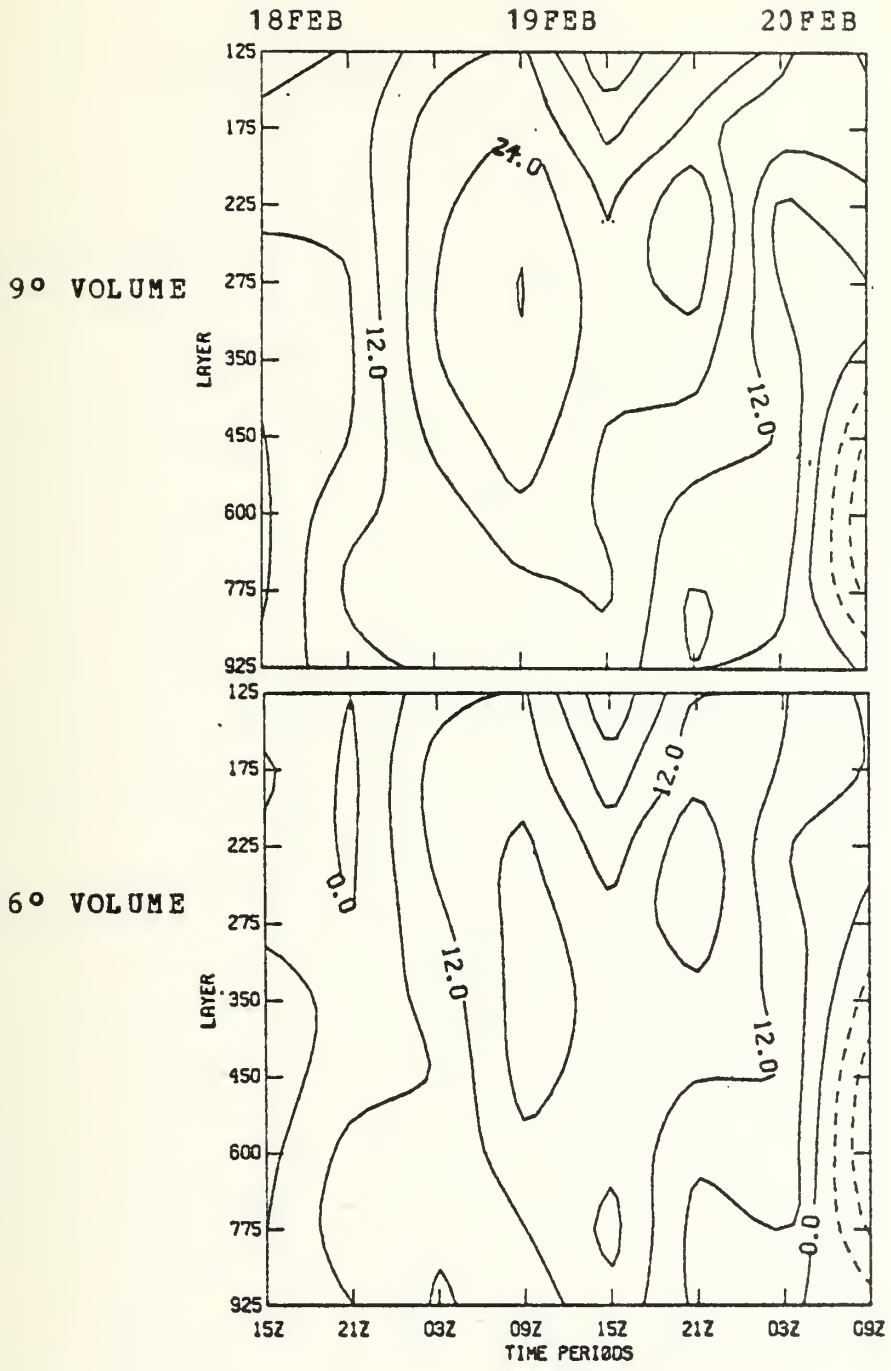

Figure 18. Absolute angular momentum time tendencies (x 10^5 cm^2 sec^{-2}). Dashed indicates negative values.

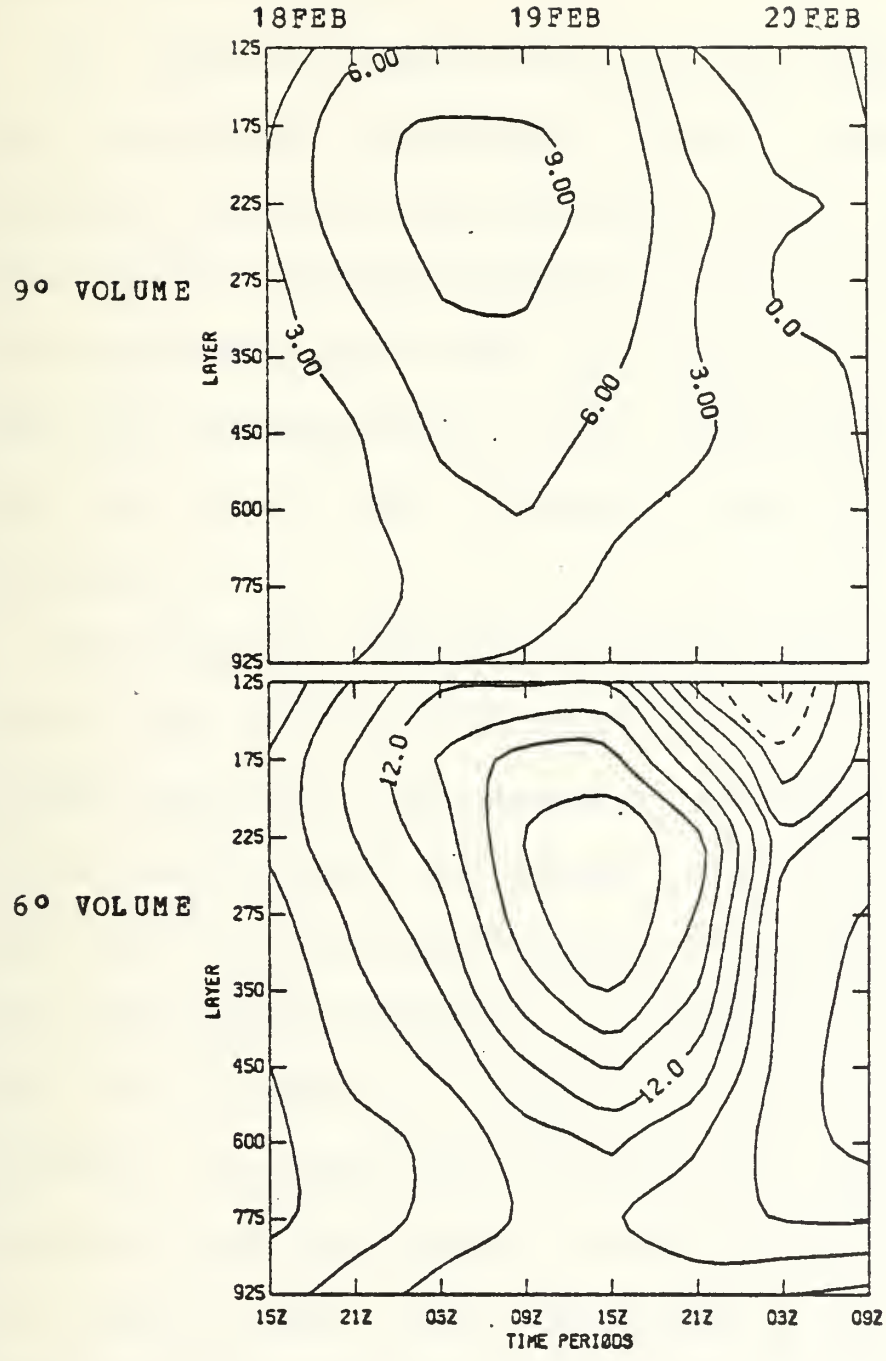

Figure 19. Absolute vorticity lateral transport (x 10^{-10} sec^{-2}). Dashed lines indicate negative values.

transport reflects transport due to the asymmetries in the cyclone and jet streak.

An alternative partitioning of the lateral transport term follows the traditional vorticity equation with the horizontal advection and divergence terms. The area-averaged absolute vorticity horizontal advection was calculated for comparison with the eddy mode transport. The divergence term was not calculated in this study and its comparison with the mean mode transport must be accomplished indirectly.

The vorticity eddy mode transport time sections (Fig. 20) are very similar to the total transport, except the magnitudes are larger. The maximum in the smaller volume again occurs during a later time period and is greater in magnitude than the outer radius maximum. The primary features in the area-averaged horizontal vorticity advection patterns (Fig. 21) generally correspond to those in the eddy mode patterns. The upper level maxima in the inner volume occur during the same time period, although the PVA maximum occurs in a higher layer. The large maximum in the upper troposphere results from the movement of the strong vorticity maximum and jet streak into the cyclone region as described

in the synoptic discussion (Figs. 7, 8, 13 and 14). The similarities in these patterns suggest a strong correlation between the eddy mode and the traditional view of the role of PVA at upper levels in the development of extratropical cyclones (Petterssen, 1956).

The most significant difference between the eddy mode and area-averaged advection patterns, particularly within the inner volume, is the PVA (approximately 15 x 10^{-10} sec^{-2}) in the 925 mb layer during the 2100 GMT 19 February period. This low-level PVA does not agree with the advection implied by the 1000mb wind vectors and absolute vorticity patterns (Fig. 12). These patterns actually indicate a net NVA within the inner radius since the wind vectors are parallel or cross the vorticity isopleths toward higher values. In an effort to resolve this discrepancy, the absolute vorticity advection values at each gridpoint were examined. The data indicate that the low-level PVA is occurring primarily at the inner radii (less than 6°) to the east and northeast of the storm center. The low-level PVA in the time sections is the result of asymmetries in the low-level vorticity contours and winds relative to the translating storm volume. The effect of the translating volume is to

enhance the low-level advecting (relative) winds (easterlies) and to reduce the upper level advecting winds (westerlies). This accounts for the smaller difference in magnitude between the upper and lower level vorticity advection maxima in a quasi-Lagrangian compared to a Eulerian budget study. Aside from these small discrepancies, the overall similarities in the patterns support the close relation between the eddy mode lateral transport and horizontal advection.

The mean mode vorticity patterns (Fig. 22) show outward lateral transport in the mid to upper troposphere and inward transport in the lower layers. These patterns reflect vorticity transport due to the low-level convergent and upper-level divergent cyclone structure. The upper-level outflow in the smaller volume increases with time to the end of the period. In contrast, the smaller maximum outflow value for the larger volume is achieved relatively early and is maintained thereafter. The larger mean mode inflow within the 6° radius volume is the result of larger vorticity values within the inner boundary as well as the more vigorous mass circulation at the inner radii.

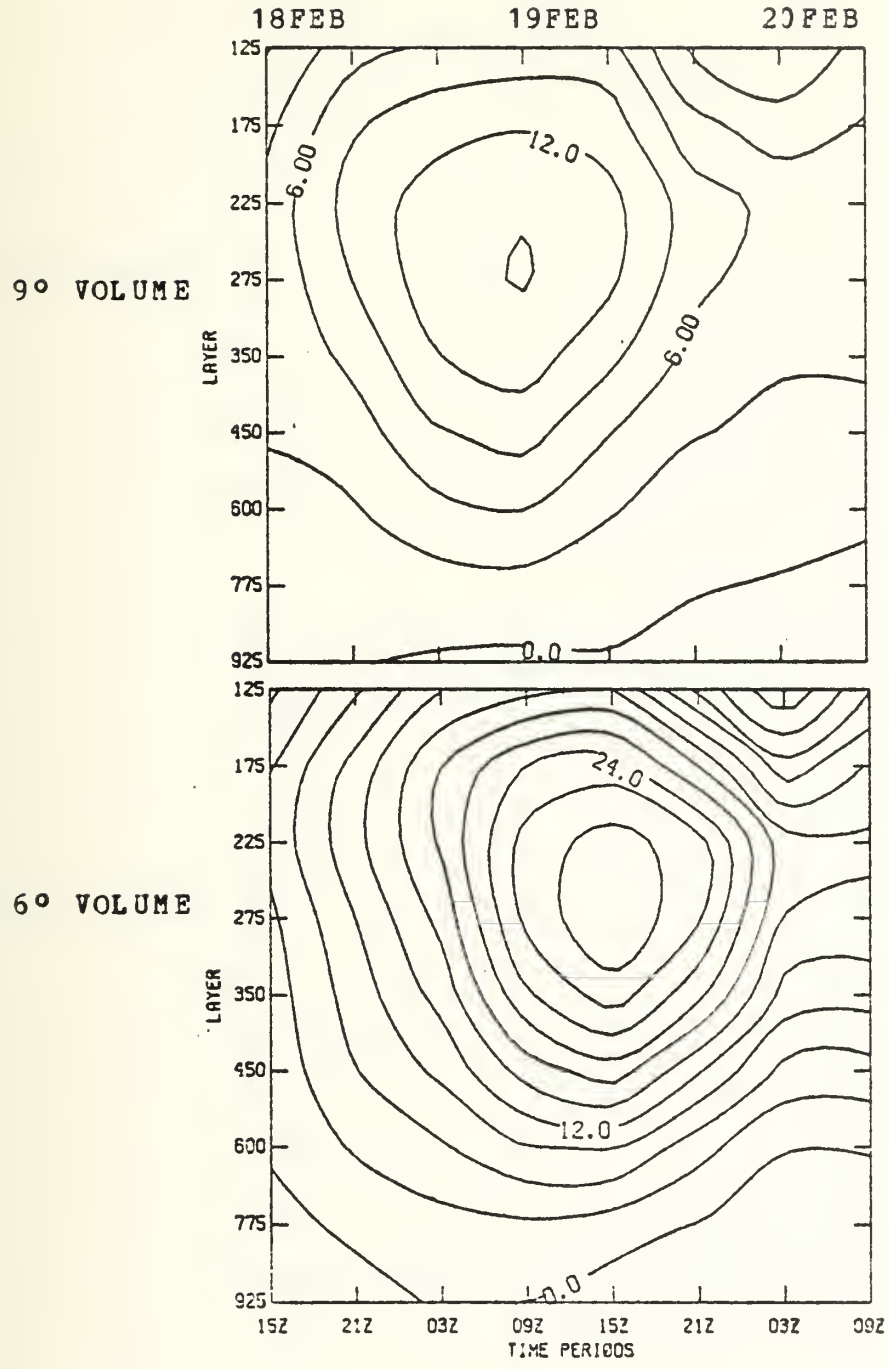

Figure 20. Absolute vorticity eddy mode lateral transport (x 10^{-10} sec^{-2}).

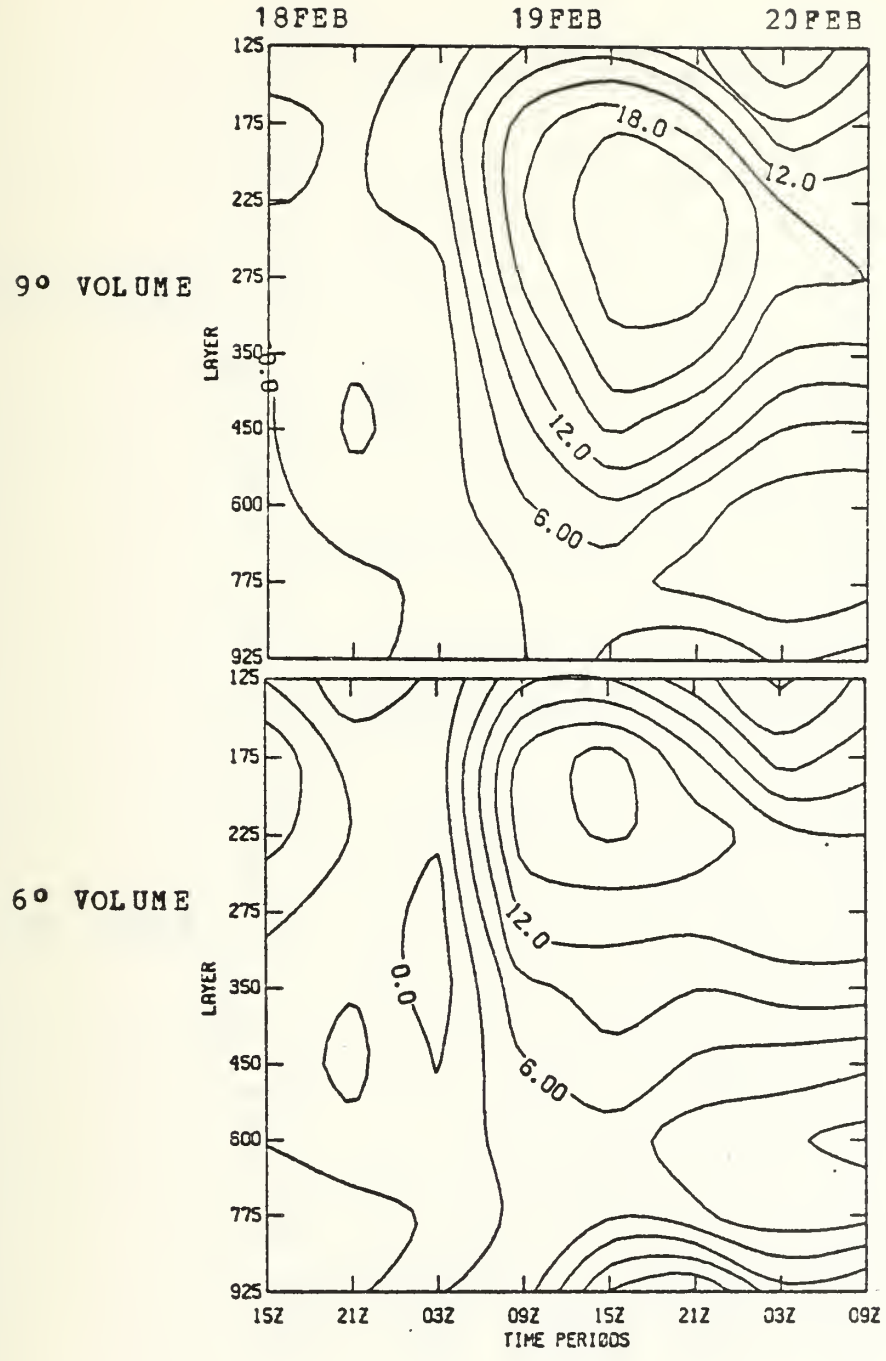

Figure 21. Areal average absolute vorticity horizontal advection (x 10^{-10} sec^{-2}).

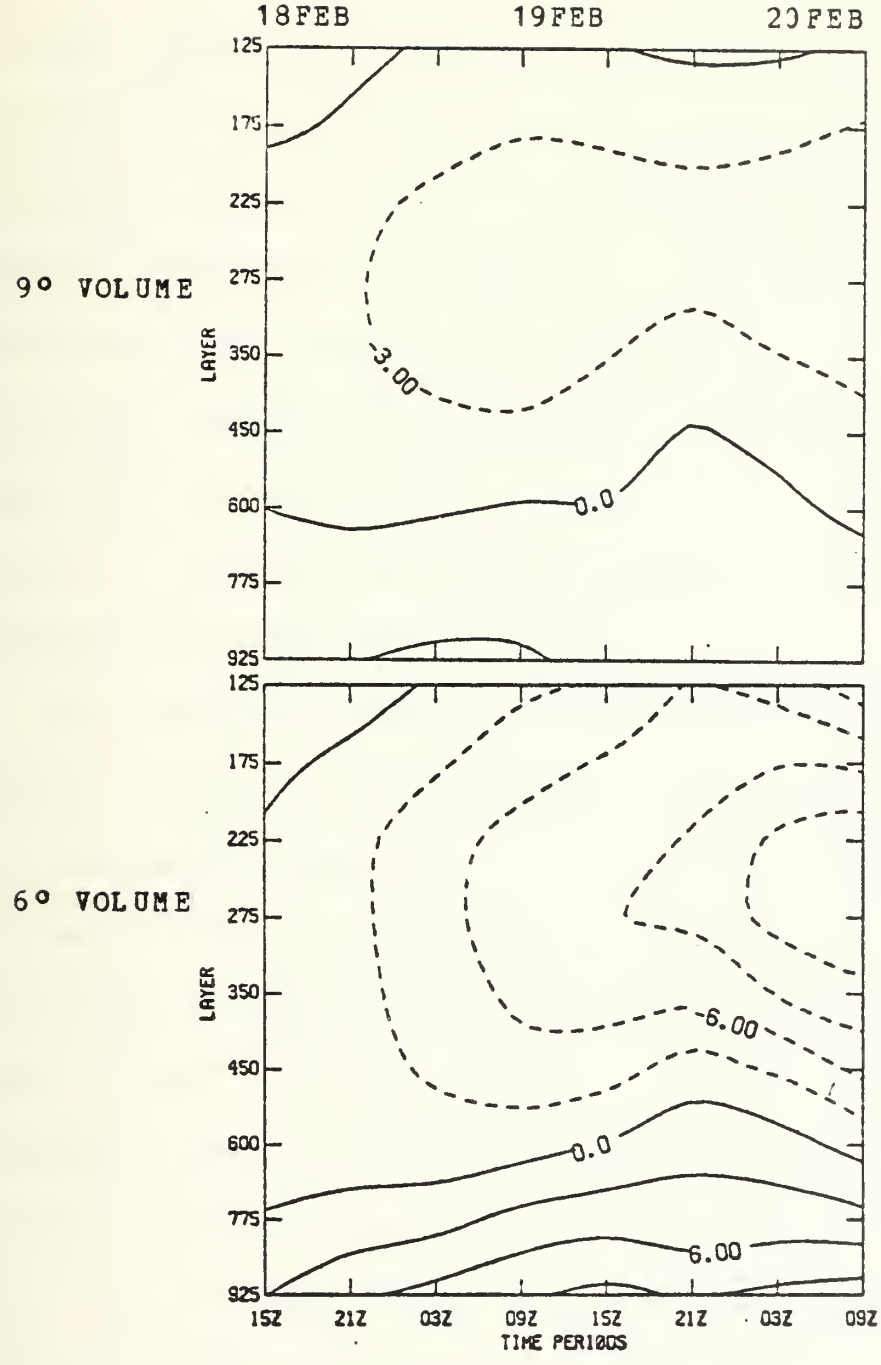

Figure 22. Absolute vorticity mean mode lateral transport (x 10^{-10} sec^{-2}). Dashed lines indicate negative values.

The vorticity lateral transport profiles (Fig. 23) illustrate the mean and eddy mode contributions to the total lateral transport. The mean mode outflow (corresponding to divergence) is overwhelmed by the eddy mode inflow (PVA) in the upper layers while, in the lower layers the mean mode inflow (convergence) dominates. The relationship between the mean mode transport and the divergence is also illustrated by noting that the level of the zero value in the mean mode profile (690mb) agrees with the mid-tropospheric level of nondivergence (LND) implied by the lateral mass transport patterns (Roman, 1981).

The absolute angular momentum lateral transport patterns (Figs. 24-26) are also similar to the corresponding vorticity patterns. Here again, the larger transport values in the outer radius are the result of the storm angular momentum values increasing with the radius. The primary difference within the inner volume is that there is outward transport in the mid to upper layers during the final time period in Fig. 24b whereas the transport is inward in Fig. 19b. This indicates that the mean mode contribution to the lateral transport is greater in the angular momentum budget than in the vorticity budget.

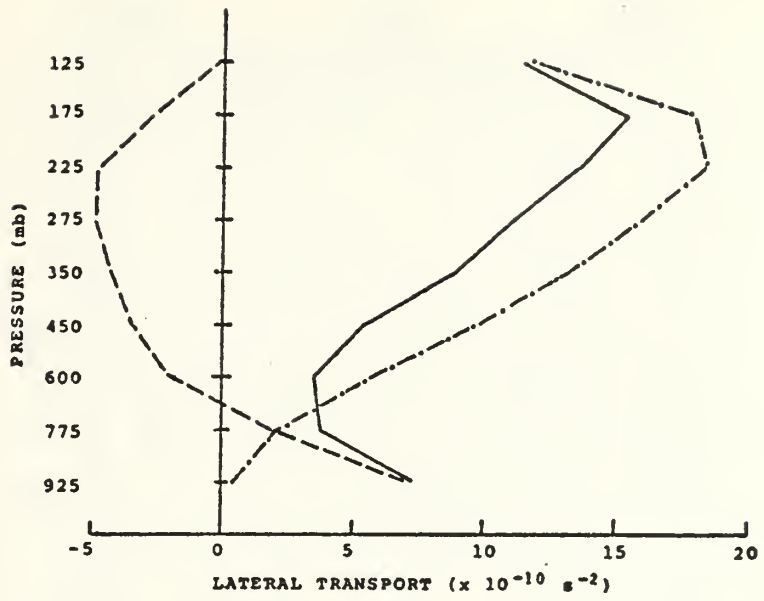

Figure 23. Total (solid), mean (dashed) and eddy (dash-dot) absolute vorticity lateral transport profiles for the 0000-0600 GMT 19 February period.

In summary, the lateral transport term is the most important term in the vorticity and angular momentum budgets. The comparisons between the eddy and mean mode partitions and the horizontal advection show that the cyclone's mean lower level inflow (convergence) forces the low troposphere vorticity and angular momentum buildup. At the upper levels, the eddy mode inward transport or horizontal advection is predominant and is responsible for the upper tropospheric increase of vorticity and angular momentum within the volume.

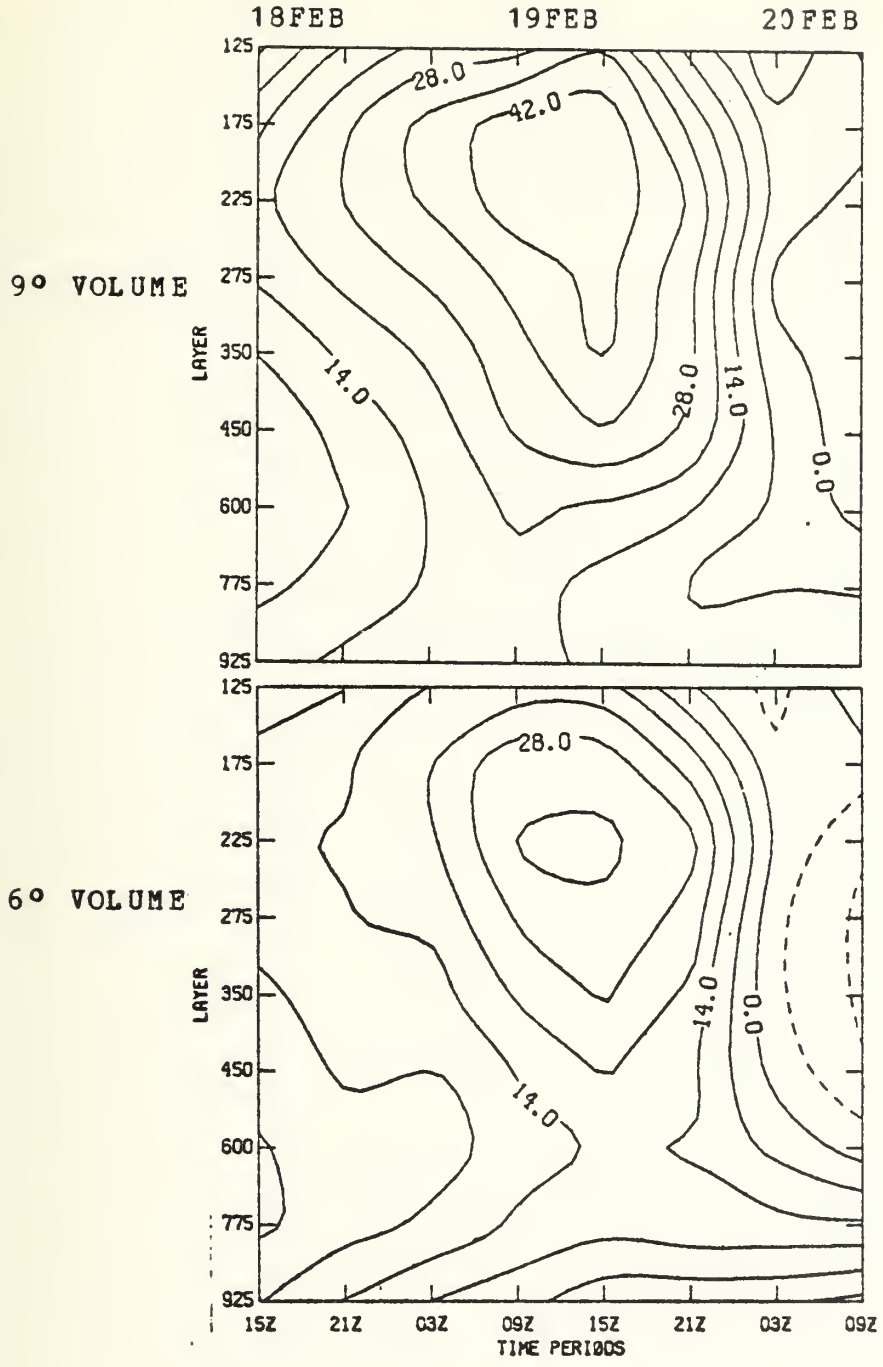

Figure 24. Absolute angular momentum lateral transport (x 10^5 cm^2 sec^{-2}). Dashed lines indicate negative values.

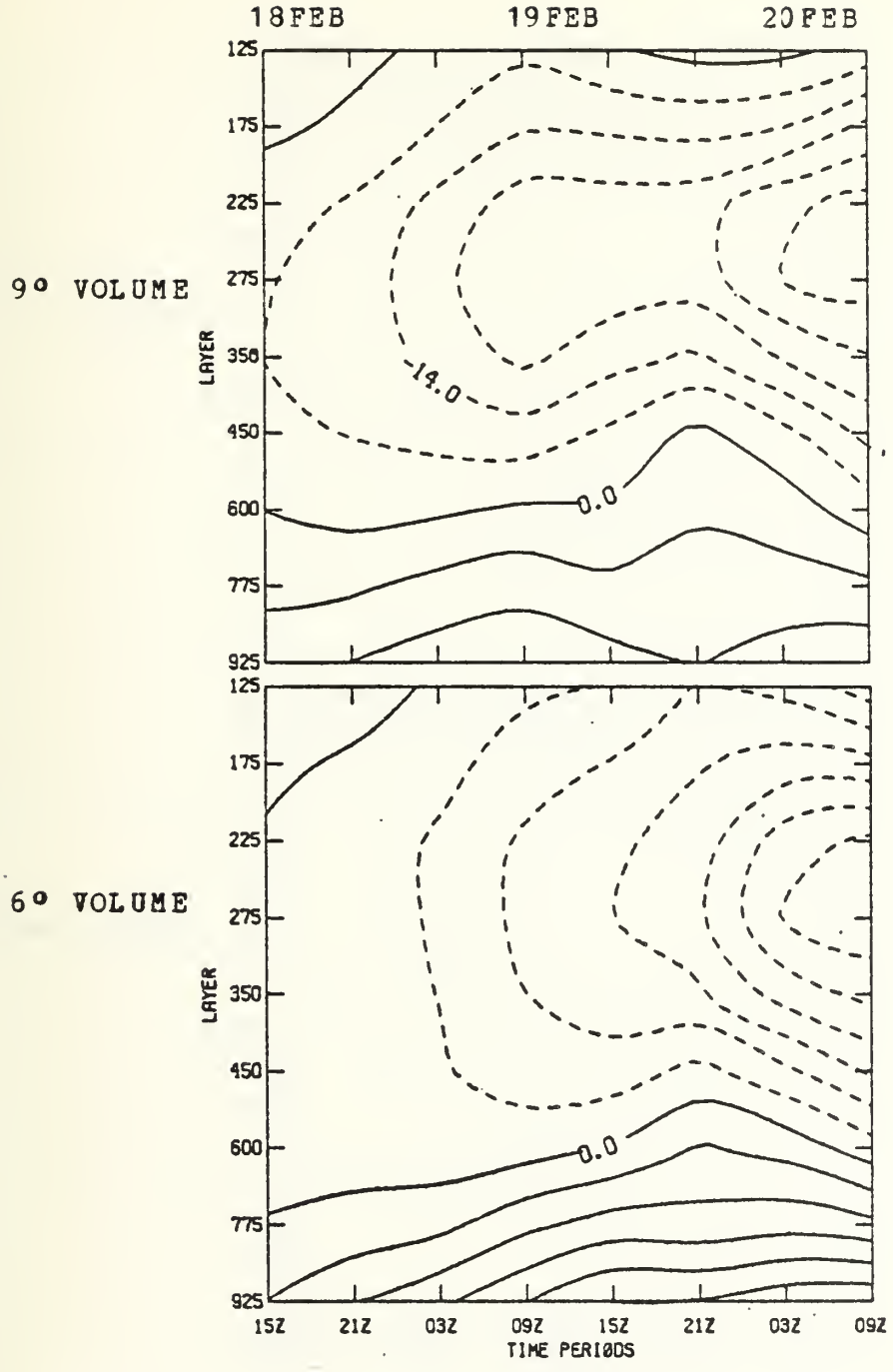

Figure 25. Absolute angular momentum mean mode lateral transport ($\times 10^5$ cm^2 sec^{-2}). Dashed lines indicate negative values.

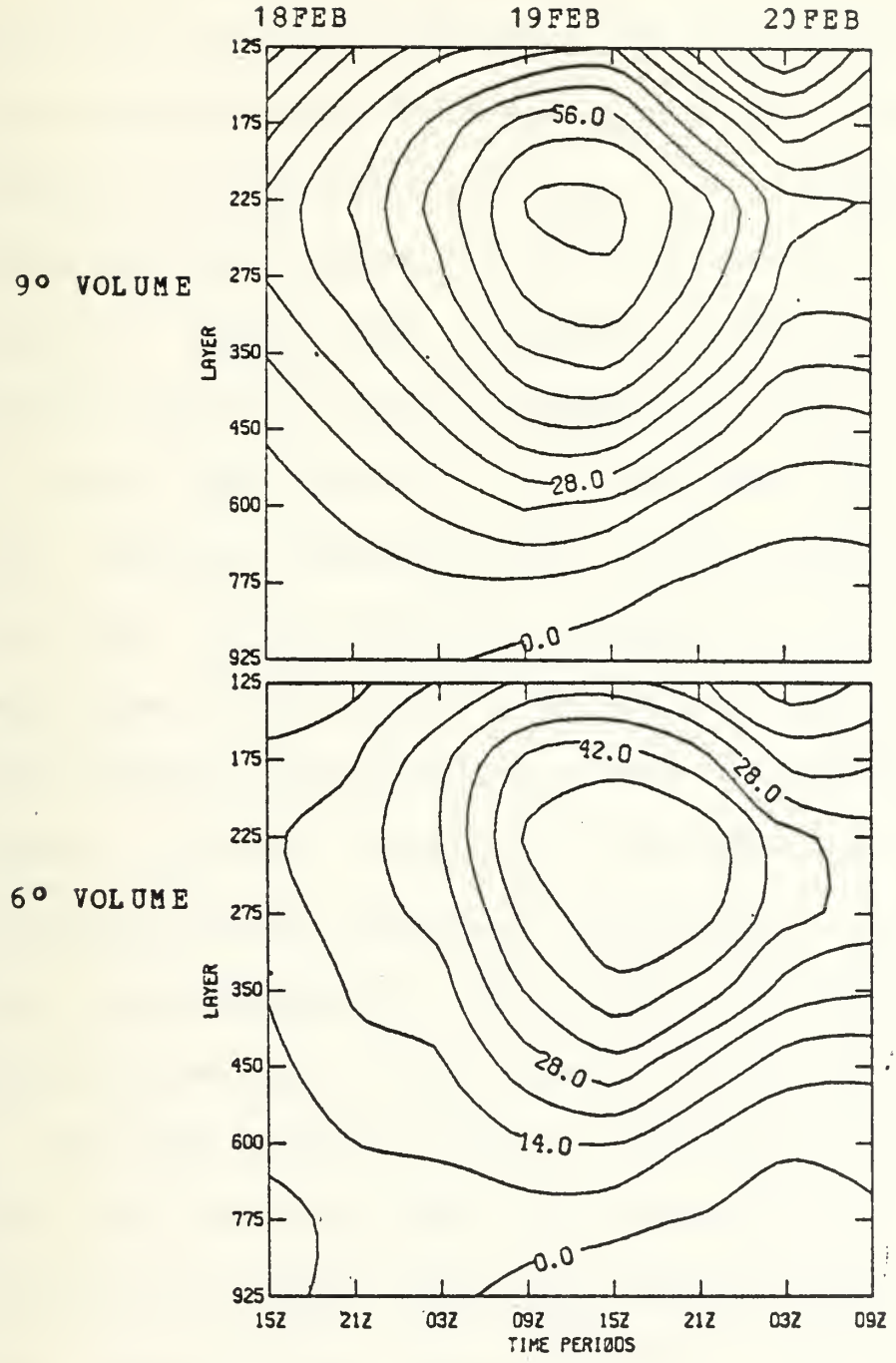

Figure 26. Absolute angular momentum eddy mode lateral transport (x 10^5 cm^2 sec^{-2}).

D. VERTICAL REDISTRIBUTION

The vertical redistribution terms (vertical vorticity advection and the divergence of the vertical angular momentum transport) were calculated using the vertical velocity fields in the FGGE data set (Fig. 27). The method used to calculate these values is briefly described in the preceding chapter. Roman (1981) calculated vertical velocities consistent with the lateral transport and time tendency terms in the QLD mass budget of the Presidents' Day Cyclone (Fig. 28); hereafter referred to as the QLD vertical velocities. Note that the QLD vertical velocities are mean values for each layer in the budget volume and can only estimate a mean mode vertical redistribution if used in the budget calculations. The time sections of the FGGE and QLD vertical velocities reveal significant differences. The FGGE values are generally greater with maximum vertical motions that occur earlier and at lower levels (600mb vice 400mb).

The FGGE vertical velocity values during the period of most rapid deepening (Fig. 29) exceed the QLD values, especially below 400mb. The discrepancy between the FGGE and mass budget vertical motion profiles is surprising. If one assumes that the FGGE vertical motions are derived from the

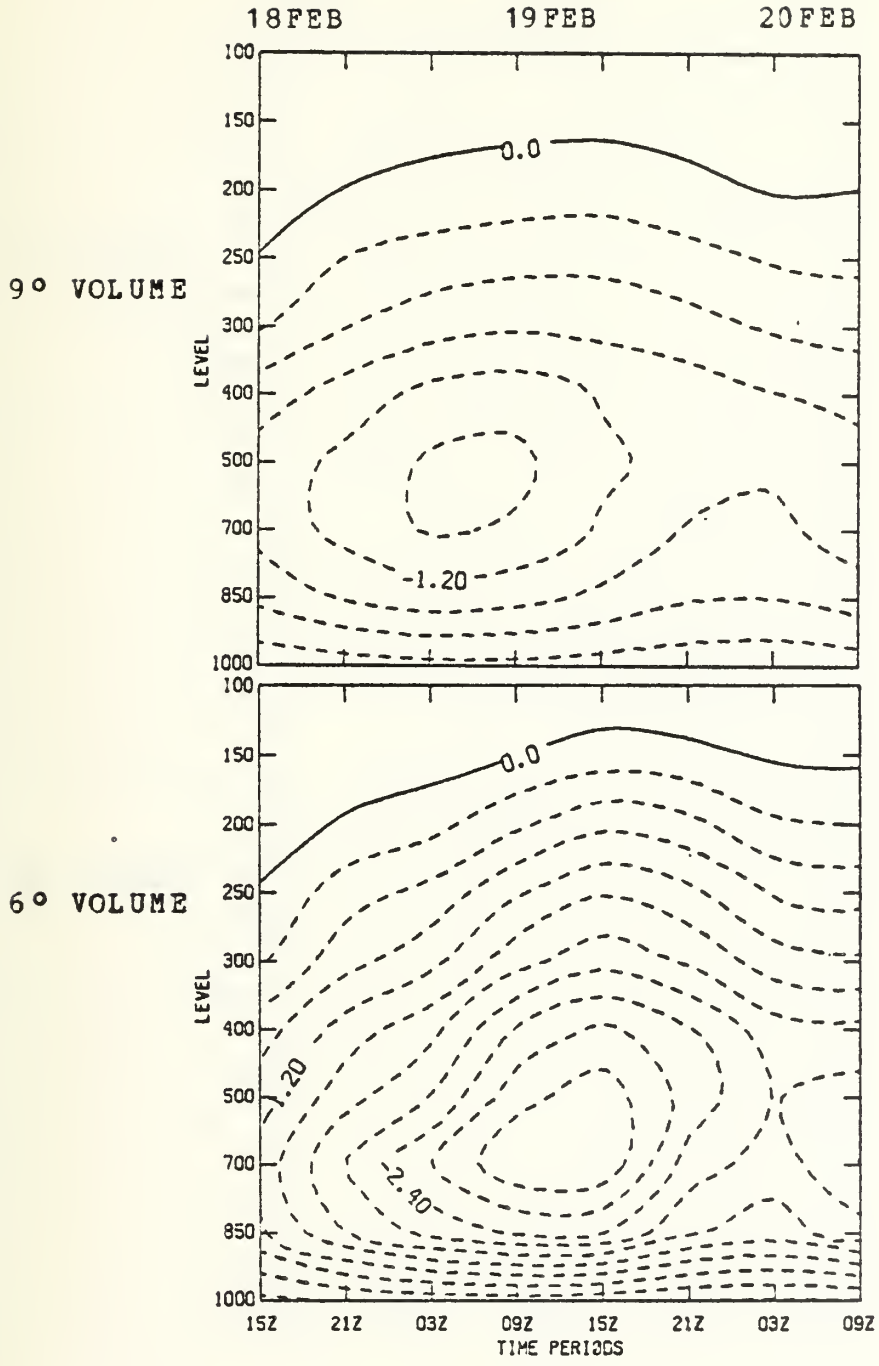

Figure 27. FGGE vertical velocity time sections (μbar sec^{-1}). Dashed lines indicate negative values.

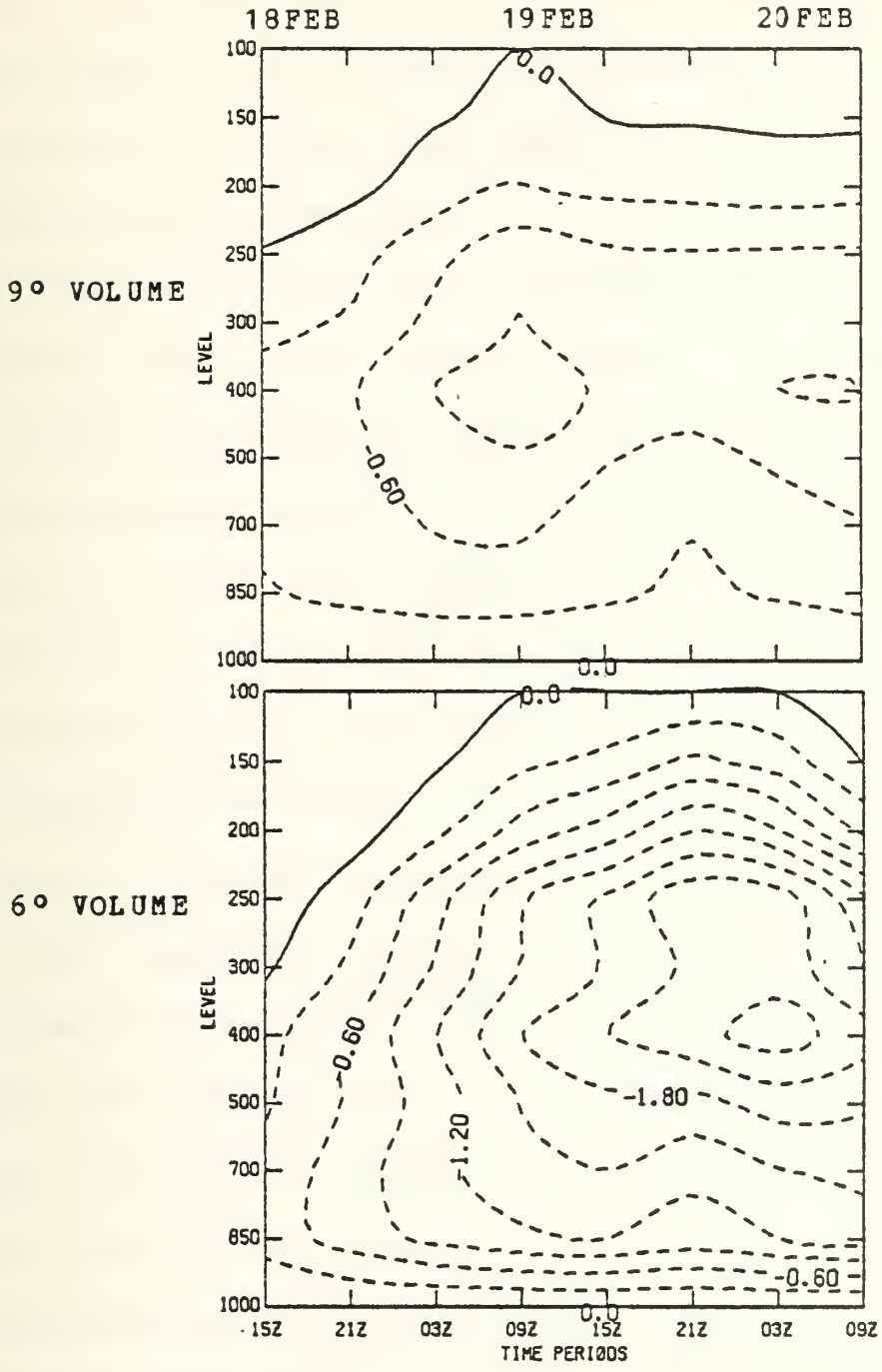

Figure 28. QLD vertical velocity time sections (μbar sec^{-1}). Dashed lines indicate negative values.

adiabatic version of the nonlinear normal mode initialization, the mass budget omegas might be expected to be larger since they include diabatic contributions. More study is required to discover the causes for these differences in vertical motion estimates.

The vertical vorticity advection time sections (Fig. 30) reveal intricate but similar patterns at each radius. Maxima occur nearly at the level of the maxima in the FGGE vertical velocity fields (used to calculate this term) but during a later time period. Weak downward advection is indicated in the mid-layers with weak upward advection in the upper layers. The mid-layer downward advection must be attributed to a reversal in the vertical vorticity gradient since no downward tropospheric vertical velocities are seen in the layer/area averaged FGGE data and a weak vorticity decrease with height is evident in the low to mid-layers in the radius six vorticity time sections (Fig. 11). The maximum value of the vorticity vertical advection term (7×10^{-10} sec^{-2}) is smaller by a factor of two than the time tendency term (13×10^{-10} sec^{-2}). These terms however, are considerably smaller than the maximum value in the total lateral transport term (25×10^{-10} sec^{-2}). Thus, the

contribution by the vertical advection term to the budget results is relatively small.

In the angular momentum budget, the vertical redistribution occurs through the vertical divergence of the vertical angular momentum transport (Fig. 31). Significant differences exist between the inner and outer volume patterns. Within radius six, a net angular momentum loss is indicated in the two lowest layers, particularly after the 0300 GMT 19 February time period. However, within the 9° volume, the pattern reveals a gain in the lowest layers and a loss in the 450mb layer during the most intense period of surface development (1200-1800 GMT 19 February). Both volumes have mid-layer gains throughout the 48-hour period, with significant gains in the upper layers in the inner volume that reach a maximum during the final period. The larger volume pattern shows a net loss in the upper layers throughout the period of study with a maximum during the 1500 GMT 19 February period.

The angular momentum vertical transport (Fig. 32) through each level was calculated to aid in resolving the primary features of the vertical divergence term. These patterns show that the maximum upward transport during the

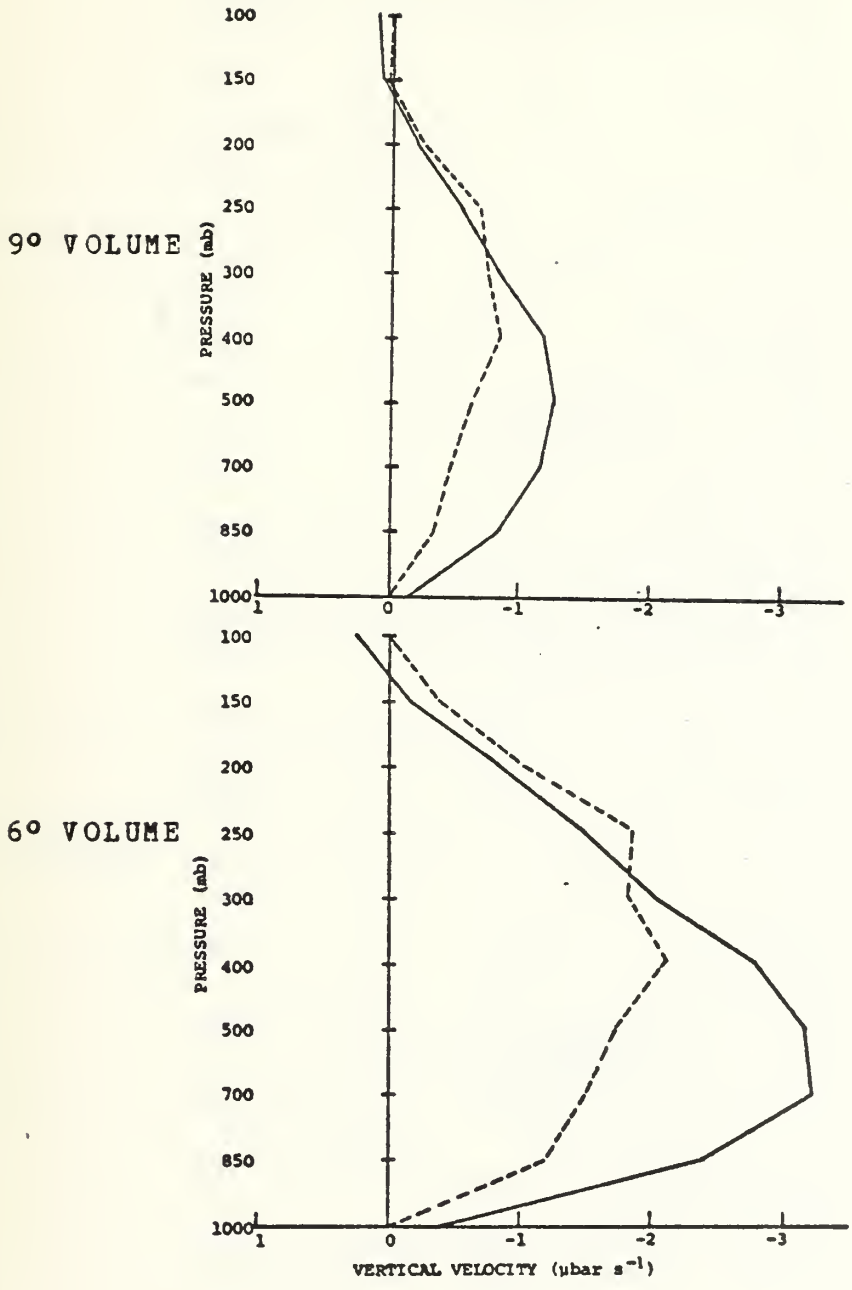

Figure 29. FGGE (solid) and QLD (dashed) vertical velocity profiles for 1200-1800 GMT 19 February 1979.

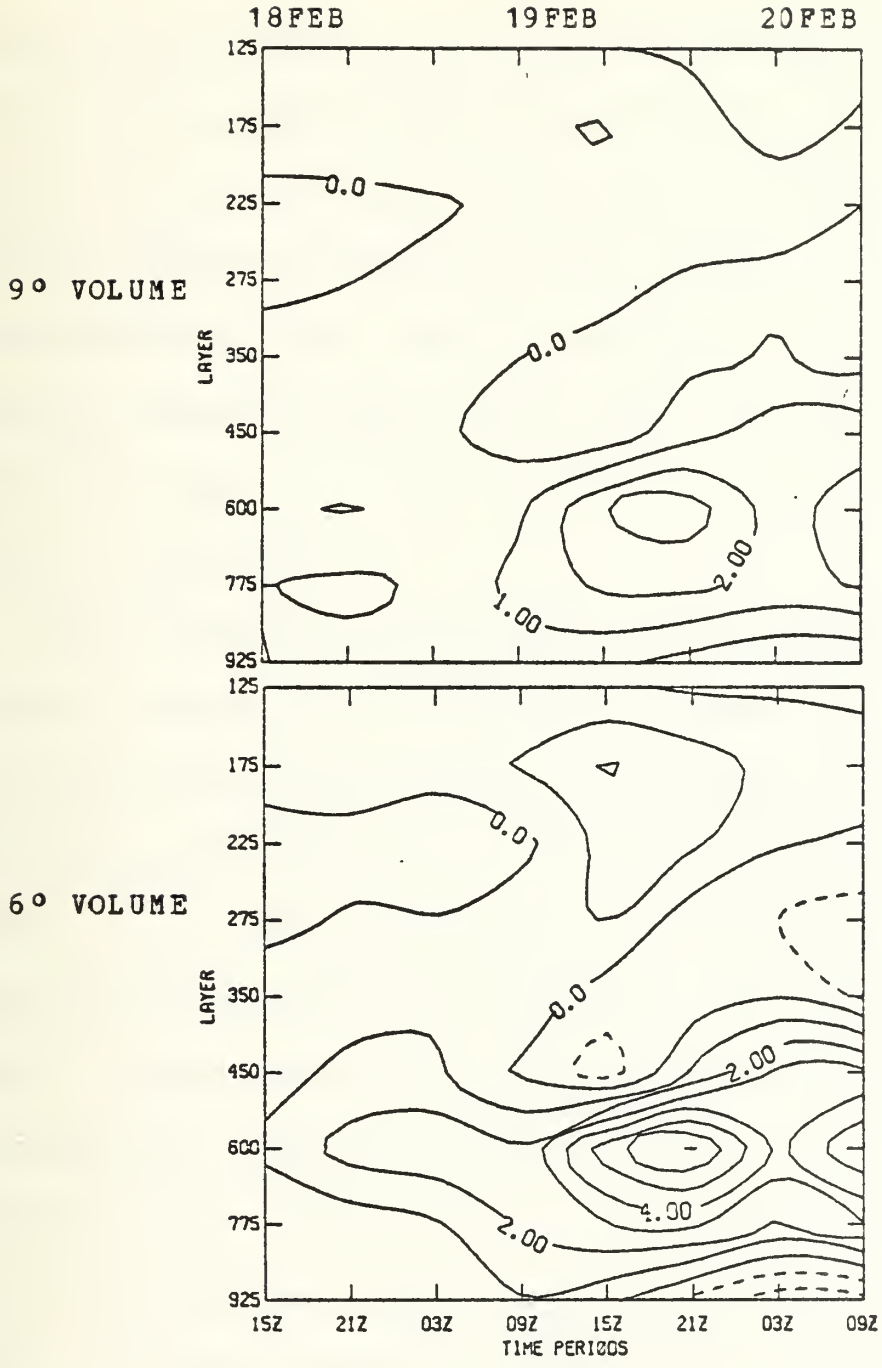

Figure 30. Vorticity vertical advection (x 10^{-10} sec^{-2}). Dashed indicates negative or downward advection.

initial time period rises from 850mb to the 700mb level by the 0900 GMT 19 February period in the 6° radius. More importantly however, is the dramatic height increase of the zero isopleth during the early stages of cyclogenesis in the inner radius. The depth of the upward angular momentum vertical transport reaches a peak during the most intense development period. Thus, a vertical divergence (loss) of angular momentum occurs in the low troposphere while a convergence (gain) of this property is found in the mid and upper troposphere.

The 9° pattern is considerably more detailed. The most striking feature is the downward transport through all levels during the 1500 and 2100 GMT 19 February periods. This indicates the presence of downward vertical velocities (not seen in the area-average omegas) in the outer radius donut. These downward values are related to the split in the maximum of area-averaged FGGE vertical velocities (Fig. 27) and the smaller vertical transport values in the outer radius compared to the inner radius. The product of the downward velocities and the larger angular momentum values at outer radii is large enough to overcome the 6° radius area-averaged upward transport and produce the downward transport in the 9° pattern during this interval.

In a general sense, the relative contribution of the vertical redistribution term (vertical divergence of the vertical transport) to the angular momentum budget can be seen by comparing maximum values. The largest value of this term in the inner volume (12×10^5 cm^2 sec^{-2}) is two thirds of the maximum inner volume time tendency term (18×10^5 cm^2 sec^{-2}). As in the vorticity budget, the lateral transport is the dominant term with a maximum value of 35×10^5 cm^2 sec^{-2} in the inner volume.

The analyses in this section have shown the upward vertical redistribution of vorticity and angular momentum from the low to the upper troposphere. In the vorticity budget, the large lower-tropospheric vorticities are advected upward although this term plays a relatively small role in the budget. In the angular momentum budget, the vertical divergence of the transport is generally negative in the lower layers and positive aloft and plays a more important role in the budget. The FGGE vertical motion estimates were found to differ significantly from the mass budget estimates.

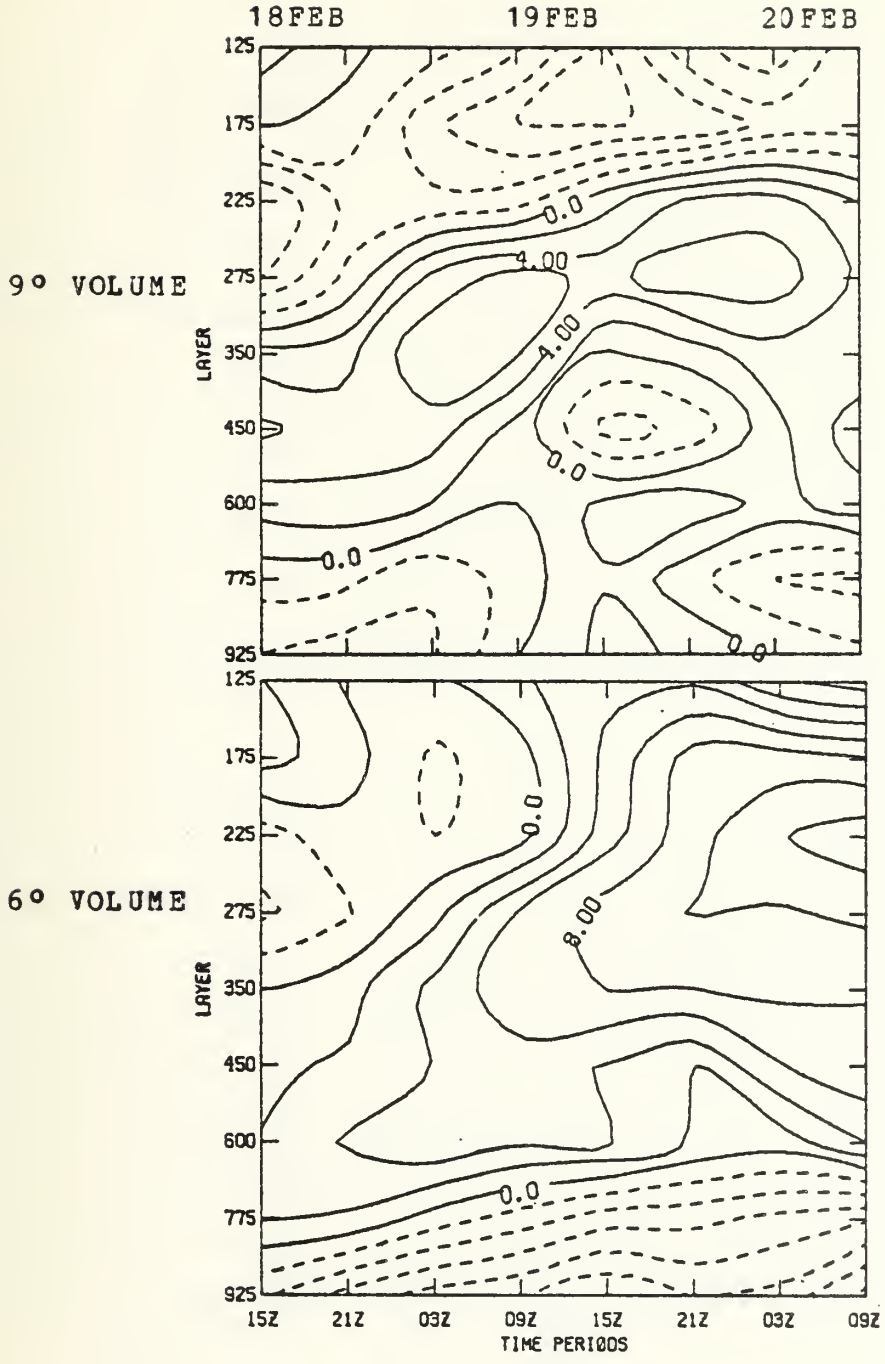

Figure 31. Divergence of absolute angular momentum vertical transport (x 10^5 cm^2 sec^{-2}). Dashed lines indicate negative values (losses).

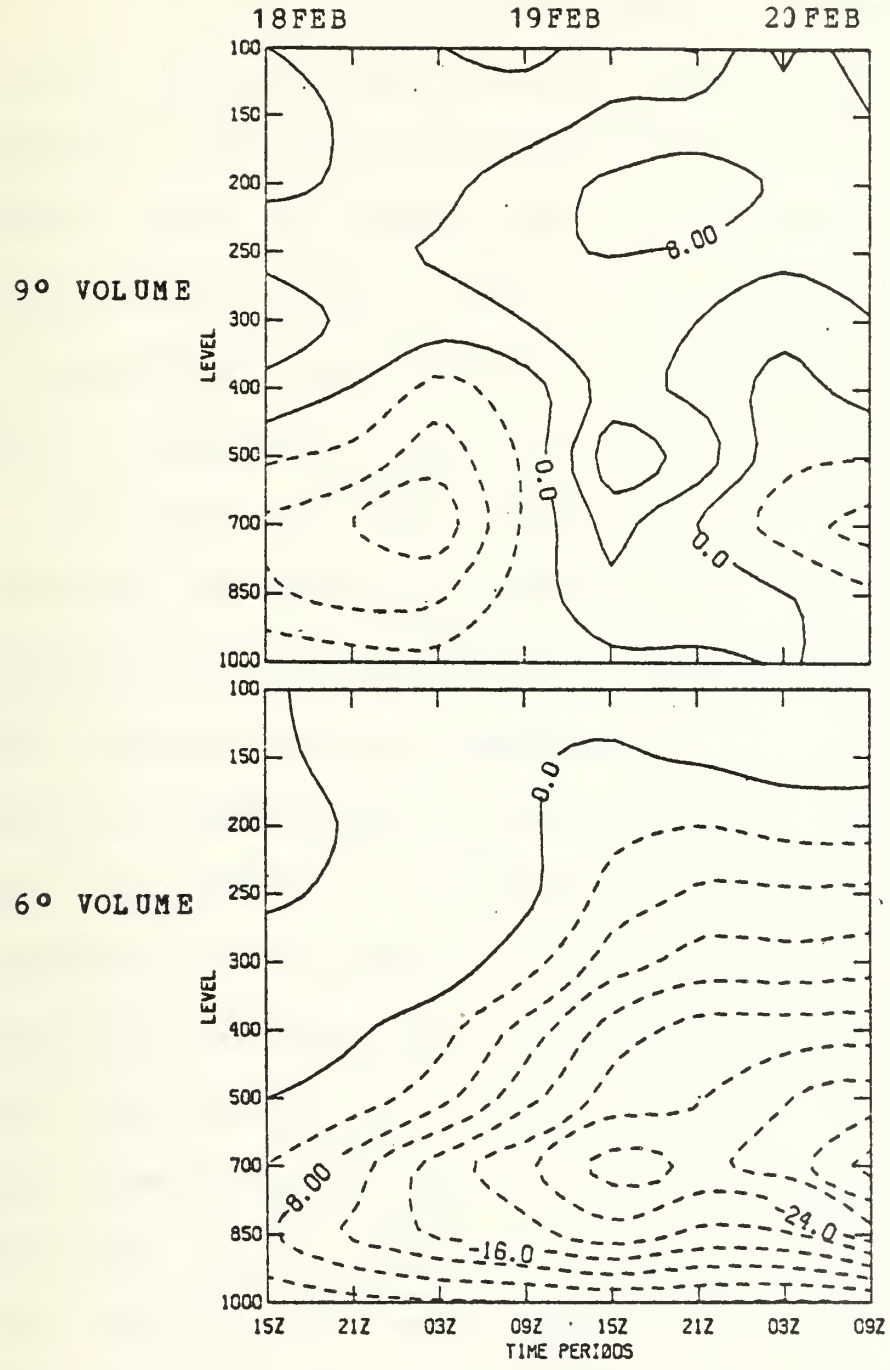

Figure 32. Absolute angular momentum vertical transport (x 10^7 mb cm^2 sec^{-2}). Dashed indicates negative values (upward transport).

E. SOURCES/SINKS

The vorticity and angular momentum sinks due to frictional dissipation were computed in the lowest layer using a stability independent parameterization scheme (Johnson and Downey, 1976) to ascertain the significance of this contribution to the budgets. The calculated values were found to be negligible compared to the other budget terms and thus have no significant effect on the budget residuals.

The vorticity tilting term (Fig. 33) was calculated and its values are generally comparable in magnitude to the time tendency and vertical advection values. The patterns show weak cyclonic vorticity generation in all layers during the early time periods and continuing in the mid-layers through the final period. Anticyclonic vorticity generation is indicated in the upper and lower layers during the 1500 and 2100 GMT 19 February time periods. Strong pattern similarities exist between the tilting and vertical advection (Fig. 30) terms during the later stages of cyclogenesis. During this time, these terms exhibit maxima of opposite sign in the lower layers and sign reversals in the mid-layers. An analysis of the components of the tilting term might reveal the reasons for the similarities and differences between the

tilting and vertical advection patterns. In this study however, the tilting term was calculated only to determine its significance relative to the primary budget terms. In any case, the tilting term patterns are consistent with the cyclone study of Chen and Bosart (1979). Overall, the patterns reveal a net positive contribution during the early stages of cyclogenesis and a net negative contribution during the latter stages.

F. RESIDUAL

Residuals were computed to determine the integrity of the budgets. The vorticity budget residuals (Fig. 34) are near zero in the lower layers within the 5° volume while in the 9° volume the values are relatively small throughout. The large negative values (a vorticity deficiency) in the upper layers in the inner volume during the 6-hour period of explosive cyclogenesis (1200 to 1800 GMT 19 Feb) deserve more intense scrutiny. The extreme value in the 225mb layer (approximately -15×10^{-10} sec^{-2}) is nearly 60% of the maximum in the total lateral transport term (nearly 25×10^{-10} sec $^{-2}$) in the inner radius. An equally large positive residual (vorticity excess) is found in the highest layer during the 0300 GMT 20 February period. Errors introduced by

interpolation, finite differencing, and spatial and time averaging can contribute to the residuals. These contributions however, should be reasonably consistent during all time periods and in all layers.

Since the largest negative residuals occur during the 6-hour period of most explosive cyclogenesis and deep convection (Bosart, 1981), it seems likely that the intense mesoscale convective processes are not adequately resolved in the FGGE data set. As in most synoptic studies, a major uncertainty lies in the vertical velocity fields. The presence of large residuals suggests that the normal mode vertical velocities (FGGE) do not explain the vertical vorticity redistribution during the period of explosive deepening.

The angular momentum budget residual patterns (Fig. 35) are more complex than the vorticity residual patterns. The major imbalances are again found during the period of intense development and convective activity, 1200 to 1800 GMT 19 February, in the outer volume. The large negative values indicate an angular momentum deficit in the mid and upper layers. Within the 6° volume, a positive maximum (excess) is found in the 350mb layer during the 0300 GMT 20 February period. However, the largest inner radius deficits

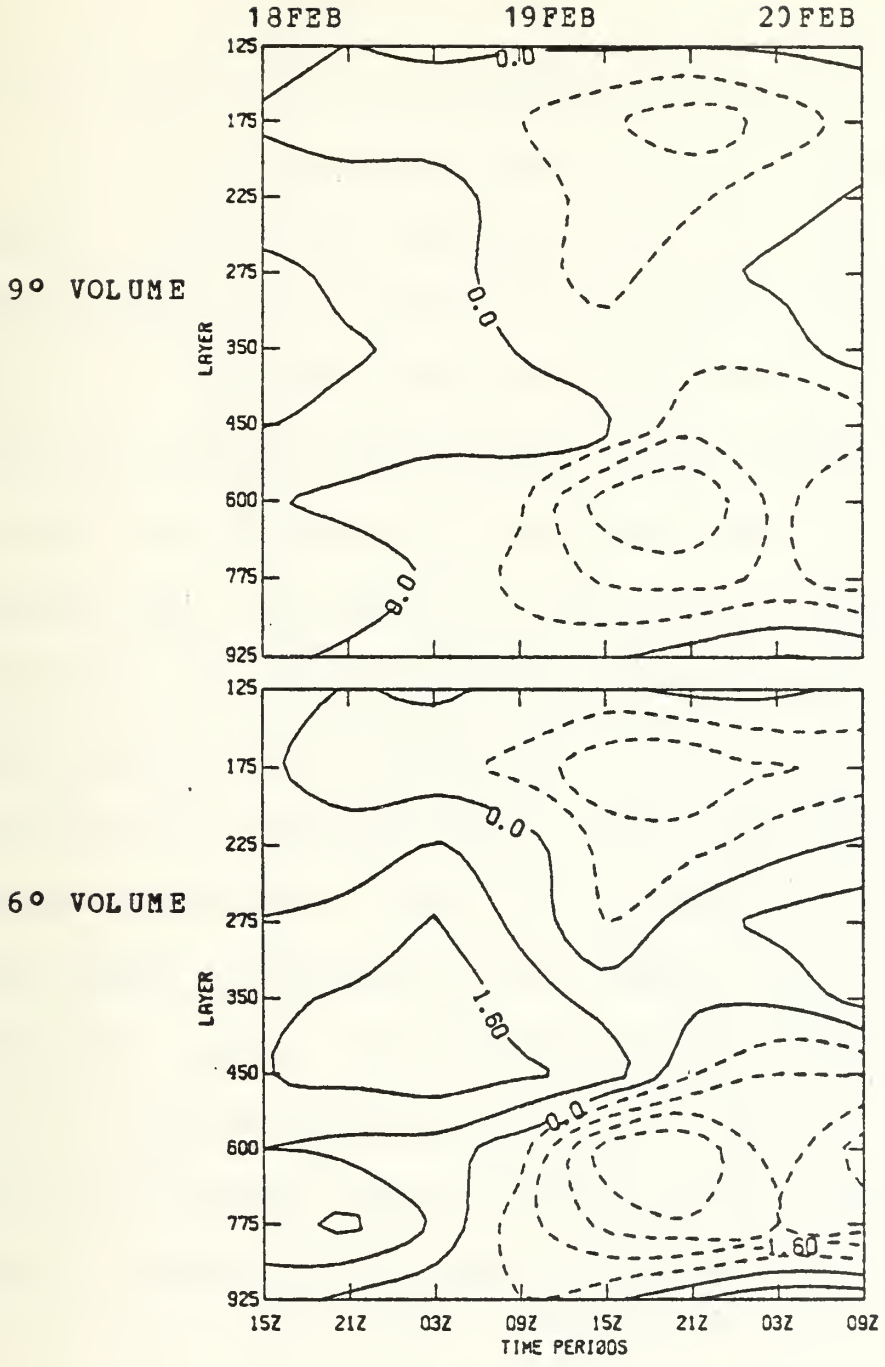

Figure 33. Tilting term in the vorticity budget (x 10^{-10} sec^{-2}). Dashed lines indicate negative values. Contour interval is 0.8 units.

are found in the lowest layers and reach a maximum during the final time period. This indicates a problem in the parameterization of the frictional torque for this data set.

An interesting point common to both budgets is that the maximum upper level deficits occur in the time interval between the double maxima in the tendency patterns (Figs. 16 and 18). At first glance this might indicate a phase problem in the budget calculations. Closer examination however, reveals that a doubling of the time tendency in the interval between the twin maxima is required to compensate for the vorticity and angular momentum deficits in the upper levels. Furthermore, this compensation would require a substantial increase in the magnitudes of the existing maxima in the tendency patterns. Thus, it is unlikely that a problem in the budget calculations is the primary cause of this inconsistency. Again, the vertical motion estimates (FGGE) used in the budget computations appear suspect, particularly since the largest deficits common to both budgets occur during the period of most rapid deepening.

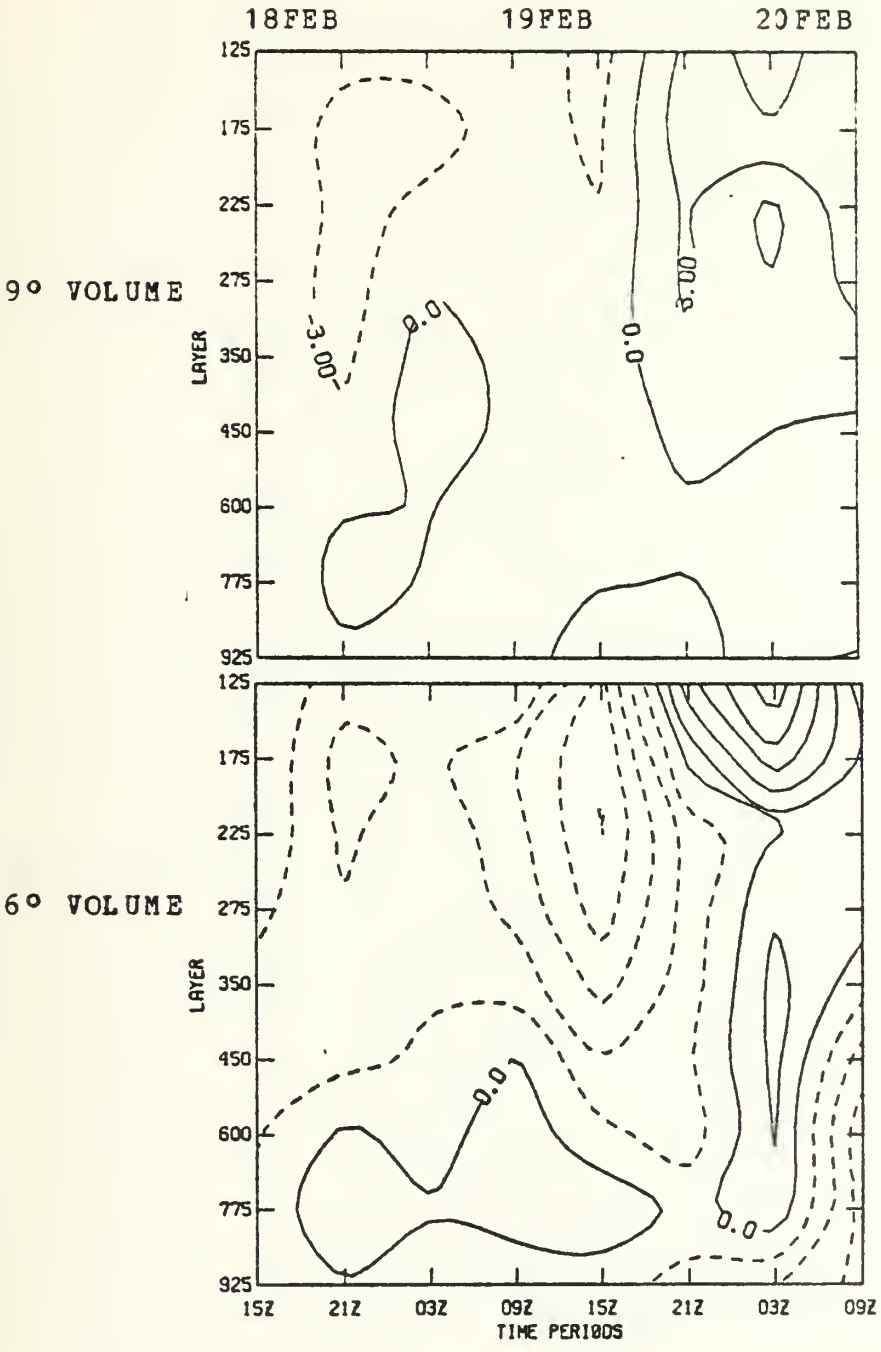

Figure 34. Vorticity budget residuals (x 10^{-10} sec^{-2}). Dashed lines indicate negative values. Contour interval is 3.0 units.

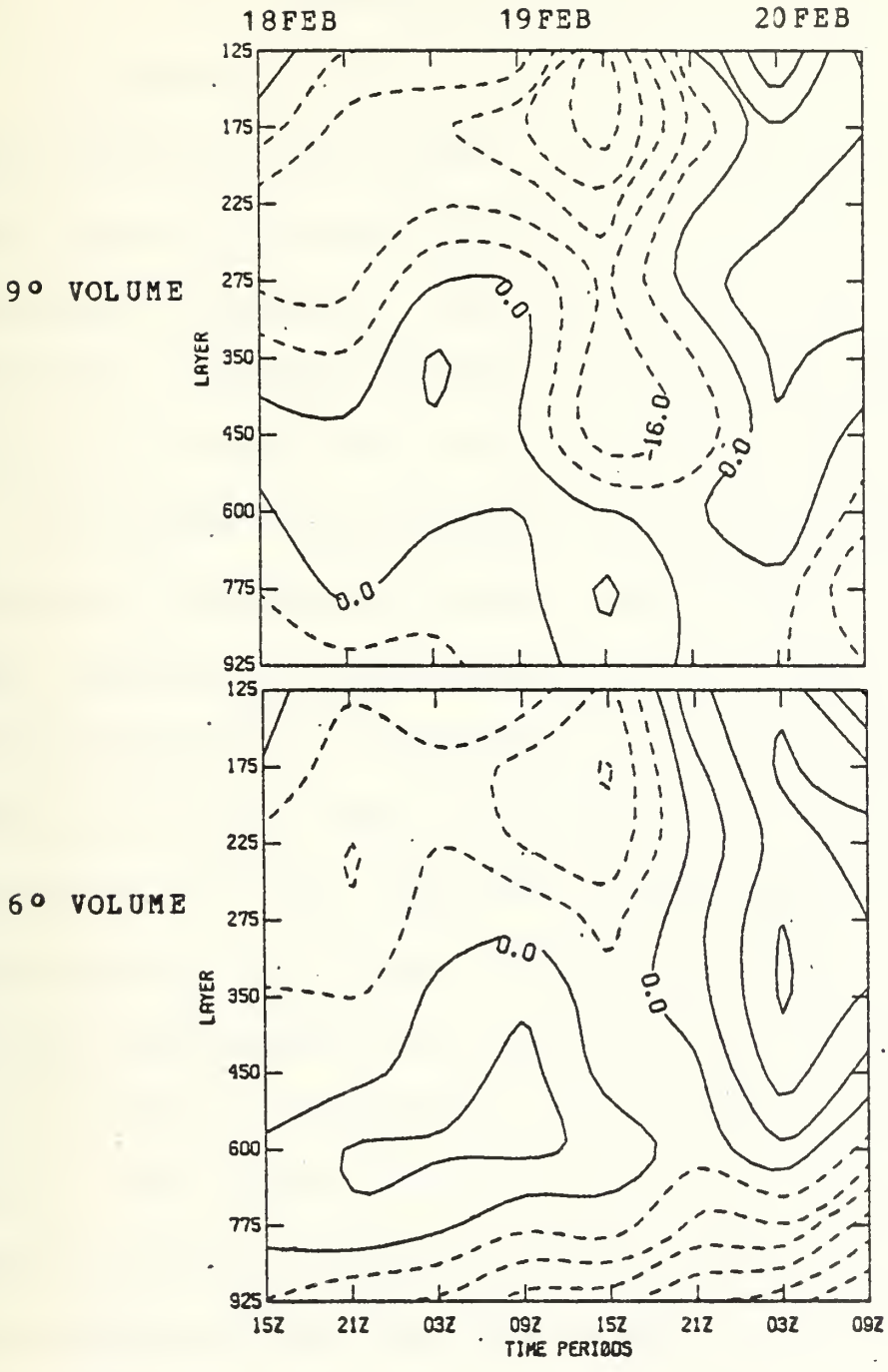

Figure 35. Angular momentum budget residuals (x 10^5 cm^2 sec^{-2}). Dashed lines indicate negative values. Contour interval is 8.0 units.

V. CONCLUSIONS AND RECOMMENDATIONS

The absolute vorticity and angular momentum budgets for the Presidents' Day Cyclone, 18-19 February 1979 were examined employing the quasi-Lagrangian diagnostic technique in pressure coordinates. The FGGE Level III-b data set prepared by the ECMWF was used to define the development and movement of the storm as well as to calculate the budgets.

The budget calculations in this study have yielded a number of interesting results. The lateral transport is the most significant term in each budget. Maximum values of the lateral transport are generally twice those of the time tendencies, which is usually the second largest term. The magnitudes of the vertical redistribution terms are approximately half those of the time tendency. The frictional dissipation was small while the vorticity tilting term is equal in magnitude to the vorticity vertical advection. The residuals in each budget were largest during the period of most intense convective activity and explosive cyclogenesis within the larger volume in the angular momentum budget and within the smaller volume in the vorticity budget.

The mass budget average vertical motion estimates were compared with the area-averaged vertical motion from the ECMWF analyses. Significant differences were found. Surprisingly, the ECMWF vertical motion estimates, which are believed to be from an adiabatic version of the nonlinear normal mode initialization, were larger than the essentially kinematic average vertical motions from the mass budget.

The mean and eddy mode partitioning of the lateral transport and the correlations with the horizontal advection and divergence components of the lateral transport show that the mean low-level inflow supplies vorticity and angular momentum to the low-troposphere. However, the upper level horizontal advection or eddy mode inward transport is primarily responsible for the absolute vorticity and storm angular momentum buildup in the upper troposphere during the development of the Presidents' Day Cyclone.

Several recommendations for further research emerged during the development of this thesis:

- Vertical velocity fields should be computed based on the FGGE Level III-b data set using the kinematic method in an attempt to incorporate the diabatic heating contribution. Calculation of the budgets based on these vertical velocity fields could then be accomplished in an effort to reduce the residuals and more accurately evaluate the budget terms;

- Vertical cross-sections of the budget terms through the storm center would allow a more detailed analysis of the large-scale dynamic forcing mechanisms;

- The divergence term of the vorticity budget should be analyzed to further understand the relationship between the advective and transport forms of the lateral transport;

- Energy diagnostics (kinetic and available potential) should also be completed on this cyclone for a more comprehensive description of the explosive cyclogenesis exhibited by this class of cyclones.

APPENDIX A

COMMON ABBREVIATIONS AND ACRONYMS

- cm centimeters
- ECMWF European Center for Medium Range Weather Forecasts
- FGGE First GARP Global Experiment
- GARP Global Atmospheric Research Program
- GMT Greenwich Mean Time
- LFM Limited area Fine-Mesh
- m meters
- mb millibars
- NVA Negative Vorticity Advection
- NMC National Meteorological Center
- PVA Positive Vorticity Advection
- QLD Quasi-Lagrangian Diagnostics
- sec seconds

APPENDIX B

QUASI-LAGRANGIAN BUDGET FRAMEWORK AND GENERALIZED BUDGET EQUATIONS

The purpose of this appendix is to present the formulation of the storm budget volume coordinate system and the generalized budget equations which can be applied to any desired atmospheric property. The information contained herein is extracted from Wash (1978) as adopted from Johnson and Downey (1975A).

Figure 36 depicts the storm budget volume in spherical coordinates. The following notation is relevant to this figure:

α	Azimuthal coordinate
β	Angular radial coordinate
$\underset{\sim}{r}$	Position vector from earth's center
$\underset{\sim}{R}$	Position vector from storm center to any point in budget volume
$\underset{\sim}{m},\underset{\sim}{l},\underset{\sim}{k}$	Orthogonal unit vectors along meridional, azimuthal and vertical directions of spherical coordinates for storm
$\underset{\sim}{U}$	Wind velocity relative to earth

$\underset{\sim}{W}_o$	Horizontal velocity of reference axis
$\underset{\sim}{W}$	Horizontal velocity at any point on the volume boundary.

Table VI contains a listing of the generalized budget equations. The following is an explanation of the notation in these equations:

$(\underset{\sim}{U}-\underset{\sim}{W})_\beta$	Horizontal wind component relative to budget volume that is normal to lateral boundary
ω	Vertical velocity in pressure coordinates
$r\sin\beta$	Radius of budget volume
p	Pressure
g	gravity

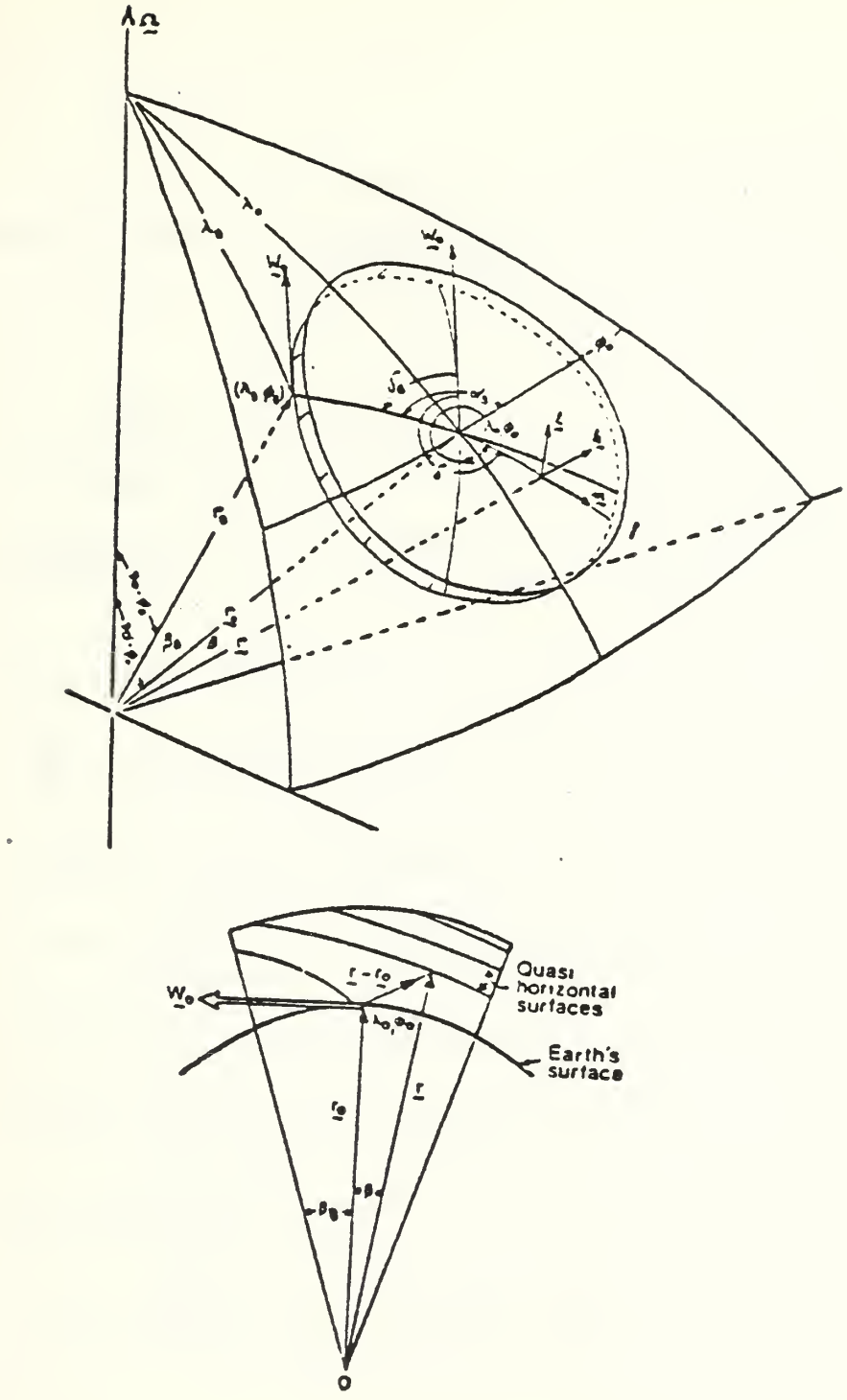

Figure 36. Quasi-Langrangian storm budget volume coordinate system (extracted from Wash, 1978).

TABLE VI

GENERALIZED QUASI-LAGRANGIAN BUDGET EQUATION IN PRESSURE COORDINATES

(after Wash, 1978)

$$F = \int_{1000mb}^{100mb} \int_{0}^{\beta} \int_{0}^{2\pi} \frac{1}{g} fr^2 \sin\beta \, d\alpha d\beta (-dp)$$

where F is the volume integral of the desired budget property f.

The budget equation is

$$\frac{\delta F}{\delta t} = LT(F) + VT(F) + S(F)$$

where the lateral transport is

$$LT(F) = \int_{1000mb}^{100mb} \int_{0}^{2\pi} \frac{1}{g} (\underset{\sim}{U}-\underset{\sim}{W})_{\beta} fr \sin\beta \, d\alpha (-dp) \Big|_{\beta}$$

and the vertical redistribution is

$$VT(F) = \int_{1000mb}^{100mb} \int_{0}^{\beta} \int_{0}^{2\pi} \frac{1}{g} \frac{\partial}{\partial p} (\omega f) r^2 \sin\beta \, d\alpha d\beta (-dp).$$

The source/sink term is

$$S(F) = \int_{1000mb}^{100mb} \int_{0}^{\beta} \int_{0}^{2\pi} \frac{1}{g} \frac{df}{dt} r^2 \sin\beta \, d\alpha d\beta (-dp).$$

LIST OF REFERENCES

Bosart, L. F., 1981: The Presidents' Day snowstorm of 18-19 February 1979: A sub-synoptic scale event. Monthly Weather Review,109, 1542-1545.

Chen, T. G., and L. F. Bosart, 1977: Quasi-Lagrangian kinetic energy budgets of composite cyclone-anticyclone couplets. J. Atmos. Sci., 34, 452-464.

Chen, T. G., and L. F. Bosart, 1979: A quasi-Lagrangian vorticity budget of composite cyclone-anticyclone couplets accompanying North American polar air outbreaks. J. Atmos. Sci., 36, 185-194.

Downey, W. K. and D. R. Johnson, 1978: The mass, absolute angular momentum and kinetic energy budgets of model generated extratropical cyclones and anti-cyclones, Monthly Weather Review, 106, 469-481.

ECMWF, 1980: The Global Weather Experiment, Daily Global Analysis, Part I.

Johnson, D. R. and W. K. Downey, 1975: Azimuthally averaged transport and budget equations for storms: Quasi-Lagrangian diagnostics 1. Monthly Weather Review, 103, 967-979.

Johnson, D. R. and W. K. Downey, 1975: The absolute angular momentum of storms: Quasi-Lagrangian diagnostics 2. Monthly Weather Review, 103, 1063-1076.

Johnson, D. R. and W. K. Downey, 1976: The absolute angular momentum budget of an extratropical cyclone: Quasi-Lagrangian diagnostics 3. Monthly Weather Review, 104, 3-14.

Kung, E. C. and W. E. Baker, 1975: Energy transformations in middle latitude disturbances. Quart. J. Roy. Meteor. Soc., 101, 793-815.

LeMoyne, J., 1982: The Ocean Ranger's night of death Newsweek, Mr 1, 99, 48.

Petterssen, S., 1956: Weather Analysis and Forecasting, Second Edition, Vol. I. McGraw-Hill, New York, Chap. 16 and 17.

Petterssen, S., and S. J. Smebye, 1971: On the development of extratropical cyclones. Quart. J. Roy. Meteor. Soc., 97, 457-482.

Roman, D., 1981: Application of Quasi-Lagrangian diagnostics and FGGE data in a study of east-coast cyclogenesis. M.S. Thesis, Naval Postgraduate School, 89 pp.

Sanders, F. and J. R. Gyakum, 1980: Synoptic-dynamic climatology of the "Bomb", Monthly Weather Review, 108, 1589-1606.

Smith, P. J., 1973: The kinetic energy budget over North America during a period of major cyclone development, Tellus, 25, 411-423.

Spaete, P., 1974: A diagnostic study of the available potential and kinetic energies of a mid-latitude cyclone. M.S. Thesis, University of Wisconsin.

Tallman, W. C., 1982: Application of quasi-Lagrangian diagnostics to to the study of numerically simulated oceanic cyclones. M.S. Thesis, Naval Postgraduate School.

Uccellini, L. W., P. J. Kocin, and C. H. Wash, 1980: The Presidents' Day Cyclone, 17-19 February 1979: An analysis of jet streak interactions, Manuscript in review.

Wash, C. H., 1975: A momentum circulation budget for an extratropical cyclone, M.S. Thesis, Department of Metecrology, University of Wisconsin, 176 pp.

Wash, C. H., 1978: Diagnostics of observed and numerically simulated extratropical cyclones, Ph.D. Thesis, Department of Meteorology, University of Wisconsin, 215 pp.

INITIAL DISTRIBUTION LIST

		No. Copies
1.	Professor Carlyle H. Wash, Code63Cw Department of Meteorology Naval Postgraduate School Monterey, CA 93940	5
2.	Professor Russell L. Elsberry, Code 63Es Department of Meteorology Naval Postgraduate School Monterey, CA 93940	1
3.	Professor Robert J. Renard, Code 63Rd Department of Meteorology Naval Postgraduate School Monterey, CA 93940	1
4.	Capt. Peter R. Conant P. O. Box 7017 Patrick AFB, FL 32925	3
5.	Capt. Alan R. Shaffer, Code 63 Department of Meteorology Naval Postgraduate School Monterey, CA 93940	1
6.	James Peak, Code 63Pj Department of Meteorology Naval Postgraduate School Monterey, CA 93940	1
7.	Professor Christopher N. K. Mooers, Code 68Mr Department of Oceanography Naval Postgraduate School Monterey, CA 93940	1
8.	Library, Code 0142 Naval Postgraduate School Monterey, CA 93940	2
9.	Commander Air Weather Service Scott Air Force Base, IL 62225	1
10.	Air Weather Service Technical Library Scott Air Force Base, IL 62225	1
11.	Commander Air Force Global Weather Central Offutt Air Force Base, NE 68113	1

12. Capt. Brian Van Orman 1
Program Manager, AFIT/CIRF
Air Force Institute of Technology
Wright-Patterson Air Force Base, OH 45433

13. Commanding Officer 1
Fleet Numerical Oceanography Center
Monterey, CA 93940

14. Commanding Officer 1
Naval Environmental Prediction Research Facility
Monterey, CA 93940

15. Commander (Air-370) 1
Naval Air Systems Command
Headquarters
Department of the Navy
Washington, D. C. 20361

16. Defense Technical Information Center 2
Cameron Station
Alexandria, VA 22314

17. Director 1
Naval Oceanography Division
Naval Observatory
34th and Massachusetts Avenue NW
Washington, D.C. 20390

18. Commanding Officer 1
Naval Oceanographic Office
NSTL Station
Bay St. Louis, MS 39522

19. Office of Naval Research (Code 480) 1
Naval Ocean Research and Development Activity
NSTL Station
Bay ST. Louis, MS 39522

20. Chairman, Oceanography Department 1
U. S. Naval Academy
Annapolis, MD 21402

21. Chief of Naval Research 1
800 N. Quincy Street
Arlington, VA 22217